

# Photoacclimation in the kleptoplastidic ciliate *Mesodinium rubrum* and its cryptophyte prey *Teleaulax amphioxeia*: phenotypic variability and implications for red tide remote sensing

Victor Pochic<sup>1,2,\*</sup> , Pierre Gernez<sup>1</sup>, Maria Laura Zoffoli<sup>3</sup>, Véronique Séchet<sup>2</sup>, Liliane Carpentier<sup>2</sup>, Thomas Lacour<sup>2</sup>

<sup>1</sup>Nantes Université, Institut des Substances et Organismes de la Mer, ISOMER, UR 2160, F-44000 Nantes, France

<sup>2</sup>Ifremer, PHYTOX, Laboratoire PHYSALG, F-44000 Nantes, France

<sup>3</sup>Consiglio Nazionale delle Ricerche, Istituto di Scienze Marine (CNR-ISMAR), 00133 Rome, Italy

\*Corresponding author: victor.pochic@univ-nantes.fr

Corresponding editor: John Dolan

## ABSTRACT

*Mesodinium rubrum* is a kleptoplastidic ciliate that sequesters the chloroplasts and nuclei of cryptophyte algae to perform photosynthesis. Blooms of *M. rubrum* can cause red tides in coastal oceans worldwide. Such red tides are detectable by remote sensing, and studying *M. rubrum* pigments and optical properties is a crucial step toward characterizing its blooms using satellite observation. Previous studies have shown that *M. rubrum* photoacclimates, modifying its pigment content depending on irradiance. Using cultures at different irradiance levels, we observed that photoacclimation in *M. rubrum* closely resembles that of its cryptophyte prey *Teleaulax amphioxeia*, leading to substantial phenotypic variability. In both species, phycoerythrin 545 cellular concentrations increased 3-fold between the highest and lowest irradiance, suggesting a major role in photoacclimation. Absorption cross-section decreased, and pigment-specific absorption coefficients increased with irradiance at the peak absorption wavelengths of chlorophyll *a* and phycoerythrin 545. After assessing the variability of absorption properties in *M. rubrum*, we combined field measurements and high-resolution Sentinel-2 satellite images to estimate chlorophyll *a* concentration of a coastal red tide and document small-scale spatio-temporal features. This work provides an overview of pigment photoacclimation in a peculiar phytoplankter and suggests guidelines for future studies of *M. rubrum* blooms.

**KEYWORDS:** *Mesodinium*; photoacclimation; phycoerythrin; bloom; remote sensing

## INTRODUCTION

*Mesodinium rubrum* Lohmann (1908) is a cosmopolitan planktonic ciliate, occurring in marine environments ranging from polar to subtropical latitudes (Moeller *et al.*, 2011; Guzmán *et al.*, 2016). High-biomass blooms of this ciliate can lead to spectacular dark red seawater discolorations, and *M. rubrum* red tides have been observed in a variety of coastal systems worldwide (Crawford, 1989). These phenomena have been documented at least since Darwin's voyage on the *Beagle*, during which he gave a striking description of a *M. rubrum* red tide and of the then unnamed animalcule that was causing it (Darwin, 1839; Hart, 1943). *M. rubrum*'s ability to form massive blooms can be surprising because this unicellular organism relies on predation for photosynthetic growth. *M. rubrum* is an obligate mixotroph that preys on cryptophyte algae and keeps their chloroplasts and nuclei inside its own cytoplasm to perform photosynthesis (Gustafson *et al.*, 2000). *M. rubrum* is capable of replicating the stolen chloroplasts during cell division, but not the stolen nucleus (kleptokaryon), and therefore needs to prey regularly

on cryptophytes to keep its photosynthetic abilities and survive (Kim *et al.*, 2017). *M. rubrum* is also known for being the prey of the kleptoplastidic dinoflagellate *Dinophysis*, a producer of toxins that can cause diarrhetic shellfish poisoning (DSP) (Park *et al.*, 2006; Minnhagen *et al.*, 2011). *Dinophysis* harmful algal blooms constitute a major threat for public health and shellfish farming in coastal areas worldwide (Díaz *et al.*, 2019; Mafra *et al.*, 2019; Guillotreau *et al.*, 2021). Studying the ecophysiology and bloom phenology of the species involved in the *Dinophysis* trophic chain is therefore crucial to better understand DSP outbreaks, anticipate and manage the risk of DSP events.

A specific trait shared by all three organisms of the *Dinophysis* trophic chain is the presence of phycobiliproteins (PBPs) in their plastids. PBPs are hydrosoluble photosynthetic pigments, only present in the plastids of cryptophytes, cyanobacteria and red algae, which play a key role in the photoacclimation of these organisms to low light environments (Zhao *et al.*, 2011; Richardson, 2022). All PBPs share the same basic molecular structure: one apoprotein linked to several chromophores, the

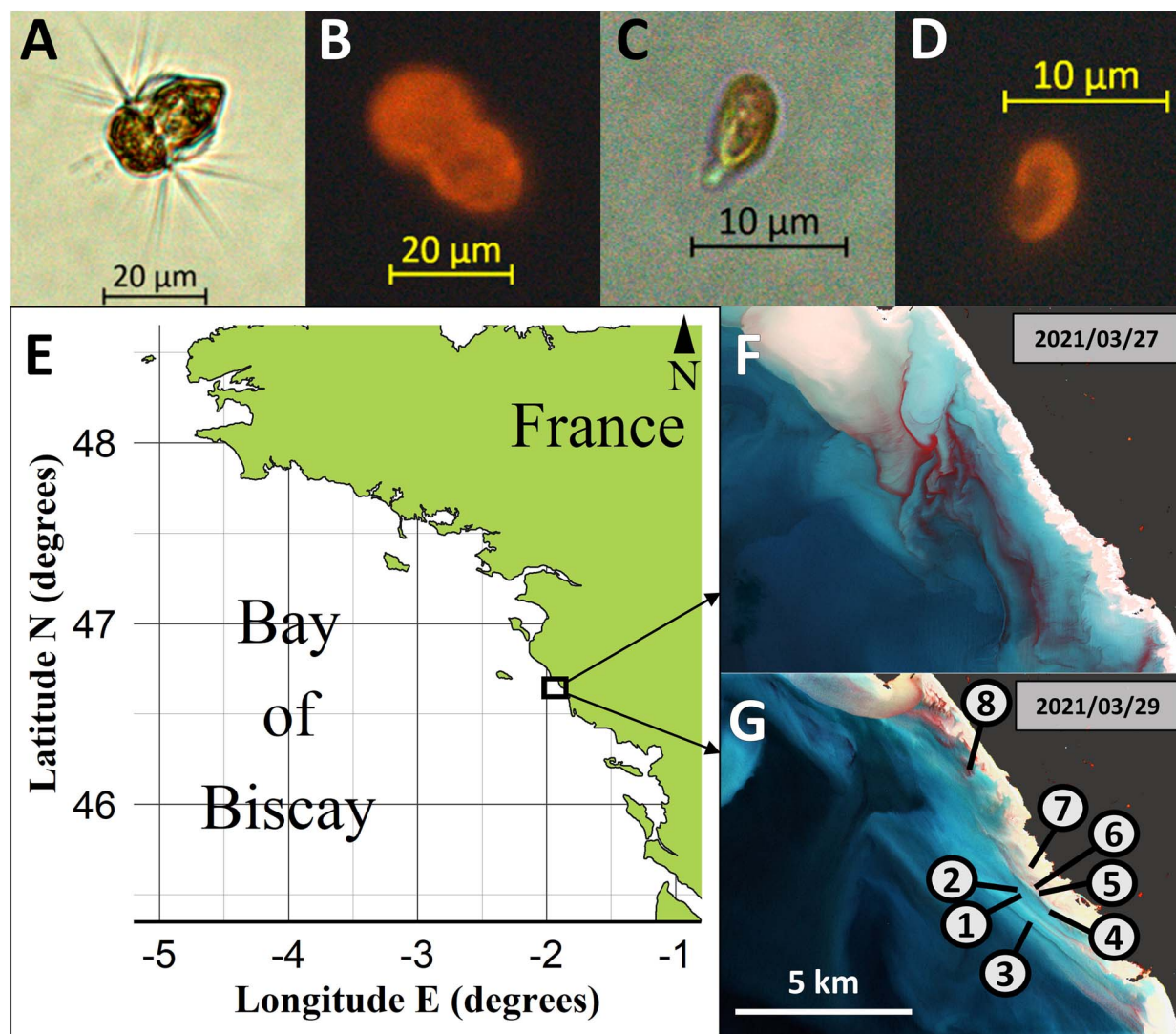


**Fig. 1.** Light microscopy photographs of *M. rubrum* (A) and *T. amphioxeia* (C). Fluorescence microscopy photographs of *M. rubrum* (B) and *T. amphioxeia* (D) showing the fluorescence of PE 545 inside the organisms (excitation wavelength: 546 nm). (E) Map of the French Atlantic coast, with the black square showing the spatial extent of the satellite images shown in (F) and (G). (F, G): False color Sentinel-2 (S2) images of a *M. rubrum* bloom, produced combining the bands 5, 3 and 2 of the S2 Multispectral Imager (MSI). The locations of eight stations sampled on 29 March 2021 are indicated in (G).

phycobilins. Nonetheless, cryptophycean PBP differ from their cyanobacterial and red algal counterparts by their quaternary structure and their cellular localization (Overkamp *et al.*, 2014). More specifically, phycoerythrin 545 (PE 545) is a major photosynthetic pigment in the cryptophyte genus *Teleaulax*, one of *M. rubrum*'s main prey (Fig. 1A–D) (Peltomaa and Johnson, 2017; Altenburger *et al.*, 2021). PE 545 is rarely quantified in studies of *M. rubrum* pigment composition (Rial *et al.*, 2013; Gaillard *et al.*, 2020), although it significantly contributes to light absorption in this organism via a broad absorption peak in the green region (475–600 nm), with a maximum at 545 nm (Barber *et al.*, 1969; Altenburger *et al.*, 2020; Gernez *et al.*, 2023). Identifying PE 545 dynamics in relation with growth conditions is therefore important for understanding the photophysiology of this ciliate.

In the dynamic ocean, planktonic organisms are exposed to multiscale variations in light exposure caused by meteorological variability, vertical mixing and variations in seawater bio-optical properties (Denman and Gargett, 1983; Lacour *et al.*, 2017). Phytoplankton are particularly effective in adjusting their metabolism to their environment which varies in irradiance intensity and spectral composition (Stramski *et al.*, 1993; Jaubert *et al.*, 2017). Photoacclimation, the ability of an algal cell to modify its metabolism—including its pigment phenotype—depending on irradiance (MacIntyre *et al.*, 2002), is a well-documented phenomenon in many taxa, including cryptophytes (Sciandra *et al.*, 2000; Laviale and Neveux, 2011; Heidenreich and Richardson, 2020). It has been established that *M. rubrum* inherits at least some photoacclimation abilities from its prey upon sequestration of their organelles. Moeller *et al.*, (2011)

have documented photoacclimation in a polar strain of *M. rubrum*, with cellular concentrations of chlorophyll *a* (chl *a*) and phycoerythrin decreasing as irradiance increases. Recent studies on photoacclimation in both *M. rubrum* and its prey showed that while the ciliate is able to photoacclimate, the precise mechanisms involved in the process are still unknown because *Mesodinium* does not display the light-dependent transcriptional changes of photosynthesis-related genes that occur in the cryptophyte (Altenburger et al., 2021; Johnson et al., 2023). In this regard, the extent to which photoacclimation in *M. rubrum* is similar to its prey remains an open question, particularly regarding its ability to adjust PE 545 concentration.

Beside its importance in eco-physiological studies, developing a better understanding of *M. rubrum* photoacclimation is of interest for optical modeling and remote sensing applications. During bloom events, dark red patches stretching over several kilometers can be detected from high-resolution satellite images due to the influence of *M. rubrum*'s PE 545 on seawater optical properties (Dierssen et al., 2015; Gernez et al., 2023). However, a detailed characterization of *M. rubrum*'s inherent optical properties is needed to develop an optical model able to unambiguously identify a bloom dominated by *M. rubrum*, and accurately assess its biomass from satellite observation (Guzmán et al., 2016). In particular, the thorough determination of *M. rubrum*'s chl *a* specific absorption coefficient, as well as its range of variability, is a prerequisite to the development of a bio-optical model that could quantitatively be used in red tide remote sensing (Craig et al., 2006; Leong and Taguchi, 2006).

In the present article, we present the results of two photoacclimation experiments. In the first one, we measured the photoacclimation response of *M. rubrum* cultures exposed to four levels of irradiance, after a 5-day acclimation period. In the second experiment, we compared the photoacclimation response of both *M. rubrum* and *T. amphioxeia*, acclimated to three levels of irradiance over a period of 12 days. From these experiments, we measured the growth rate, absorption coefficient and pigment content of both species, including the hydrosoluble phycoerythrin 545. We compared the absorption coefficients and pigment compositions measured on cultures to field and laboratory data from the literature, and to that of field samples acquired during a red tide of *M. rubrum*. Then, we assessed the influence of the range of variability in *M. rubrum*'s chl *a*-specific absorption coefficient on chl *a* estimation using a standard remote-sensing algorithm (Gons et al., 2002). Finally, we computed maps of chl *a* concentration during a bloom of *M. rubrum* observed at high spatial resolution with the Sentinel-2 satellite mission. These maps allowed us to document small-scale features of the bloom surface distribution, as well as its rapid temporal evolution.

## METHODS

### Photoacclimation experiments

*Teleaulax amphioxeia* (strain AND-A0710, 2007, Huelva, Southwestern Spain) and *M. rubrum* (strain MrDK-2009, 2009, Helsingør harbor, Denmark) cultures were grown in 35 mL of prefiltered L1 medium (Guillard and Hargraves, 1993), in 50-mL glass Erlenmeyer flasks. Two independent experiments were conducted. In the first one, *M. rubrum* cultures were maintained at 17.5°C, under 12/12 h light/dark illumination,

provided by white fluorescent tubes (Fig. S1) at 20, 65, 120 and 220  $\mu\text{mol photons.m}^{-2}.\text{s}^{-1}$ , as measured with a LI-250A Light Meter (LI-COR Biosciences) in air mode. The kleptoplastic ciliate *M. rubrum* was fed with *T. amphioxeia* (grown at 17.5°C and 65  $\mu\text{mol photons.m}^{-2}.\text{s}^{-1}$ ) on day 0, at a prey-predator ratio of 3:1. This first photoacclimation experiment lasted for 5 days, at the end of which cultures were sampled for analysis. In the second experiment, semicontinuous cultures of *T. amphioxeia* and *M. rubrum* were grown at 21°C, in a 12/12 h light/dark cycle at irradiances of 20, 80 and 200  $\mu\text{mol photons.m}^{-2}.\text{s}^{-1}$ . The acclimation period lasted for 12 days, during which *M. rubrum* was fed with *T. amphioxeia* (grown at 20  $\mu\text{mol photons.m}^{-2}.\text{s}^{-1}$ ) every 3 days at a ratio of 3 prey cells for 1 predator. Cultures were sampled for analysis at the end of the acclimation period.

During the first experiment, cell counts and equivalent spherical diameter (ESD) of the microalgal cells were monitored at the start (day 0) and at the end (day 5) of the experiment, with a particle counter (Multisizer 3, Beckmann-Coulter). During the second experiment, cell counts, chl *a* fluorescence and PE 545 fluorescence were monitored daily with a flow cytometer (MACSQuant 10, Miltenyi Biotec), while ESD of the cells were measured with the particle counter on the final day of the experiment. Daily monitoring confirmed that cryptophytes were promptly consumed by the ciliates, within a day after the feeding. In cultures of *M. rubrum* at 80 and 200  $\mu\text{mol photons.m}^{-2}.\text{s}^{-1}$  at 21°C, a contamination of the cultures by small-sized brown microalgae was identified by an unexpected population of relatively small, chl *a*-containing cells in the cytograms and confirmed by the detection of the carotenoids fucoxanthin and diadinoxanthin/diatoxanthin in these cultures (Fig. S2). The low concentration of contaminating cells (<7% of total cell biovolume) is unlikely to have significantly influenced the photophysiological response of *M. rubrum*. Predation of *M. rubrum* on these contaminating brown algae is also unlikely due to its strict prey selectivity toward certain cryptophytes (Peltomaa and Johnson, 2017). However, we cannot rule out the fact that some slight allelopathic effects from the brown algae toward the ciliate influenced the latter's physiology. We need to consider nonetheless that because of this contamination, the concentrations of chl *a* and chl *c*<sub>2</sub> attributed to *M. rubrum* in these cultures were slightly overestimated. Occasional contaminations of *M. rubrum* cultures by the small chrysophyte *Ochromonas sp.* were reported by Hernández-Urcera et al. (2018). Although the contaminating algae in our study were not *Ochromonas* (no violaxanthin/zeaxanthin detected), it testifies to the difficulty of growing pure cultures of *M. rubrum* in undiluted culture medium.

The relationship between the growth rate ( $\mu$ , d<sup>-1</sup>) and growth irradiance ( $E$ ,  $\mu\text{mol photons.m}^{-2}.\text{s}^{-1}$ ) was modeled by fitting to the data the following equation, as suggested by MacIntyre et al. (2002):

$$\mu = \mu_m \left( 1 - \exp\left(\frac{-E}{K_E}\right) \right) \quad (1)$$

where  $\mu_m$  is the maximum growth rate (in d<sup>-1</sup>) and  $K_E$  is the light saturation parameter for growth (in  $\mu\text{mol photons.m}^{-2}.\text{s}^{-1}$ ). The relationship was fitted to the data by nonlinear least-squares.

For the measurement of lipophilic pigments and absorption coefficients, samples were filtered onto 0.7- $\mu\text{m}$  pore glass fiber filters (Whatman, grade GF/F) and stored at  $-80^\circ\text{C}$ . For PBP measurements, samples of cultures were centrifuged at 4100 g for 10 minutes. A cell count was performed on the supernatant after the centrifugation to assess the proportion of cells that were missing in the pellet. The pellets were then stored at  $-80^\circ\text{C}$ . For the second experiment only, 5 mL of each culture were sampled for *in vivo* absorption measurements that were done within 4 hours after sampling.

### Extraction and quantification of lipophilic pigments

Filters sampled for pigment analysis were immersed into 2 mL of 95% acetone, sonicated for 10 minutes in an ultrasonic water bath (Advantage Lab) and thawed at  $-20^\circ\text{C}$  for 24 h. Extracts were then filtered onto a 0.2- $\mu\text{m}$  pore PTFE membrane filter (Whatman), before injection in high performance liquid chromatography (HPLC). The concentrations of lipophilic pigments in the extracts were measured by HPLC-UV-DAD (series 1200; Agilent Technologies) using an Eclipse XDB-C8 reverse phase column (150 mm  $\times$  4.6 mm, 3.5  $\mu\text{m}$  particle size; Agilent Technologies). For one condition (*M. rubrum*,  $17.5^\circ\text{C}$ ,  $65 \mu\text{mol photons.m}^{-2}.\text{s}^{-1}$ ), the sample of one replicate was degraded, and the resulting pigment concentrations were uninterpretable.

### Extraction and quantification of phycoerythrin 545

PBPs were extracted following the protocol recommended by Lawrenz *et al.* (2011). The pellets were unfrozen and suspended in 4 mL of 0.1 M Na-phosphate buffer (pH = 6.3; Gomori, 1955), sonicated for 10 minutes, then left to thaw at  $4^\circ\text{C}$  for 24 h. The extracts were then centrifuged (4100 g, 10 minutes). For each sample, a volume of 200  $\mu\text{L}$  of supernatant, containing the extracted PE 545, was filtered on a 0.2- $\mu\text{m}$  pore polyethersulfone (PES) filter to eliminate minute cell parts containing lipophilic pigments. The optical density (OD) of the filtered supernatant was then measured from 400 to 750 nm with a 96-well plate-reading spectrophotometer (Tecan, Infinite200Pro). The solution of phosphate buffer used for the extraction was taken as reference. The value of OD at 750 nm was subtracted throughout the spectrum as correction, because the absorption of PE 545 is null in the near-infrared spectral range. The concentration of PE 545 ([PE 545], in  $\text{mg.L}^{-1}$ ) was calculated from the OD at the peak of absorption at 552 nm using an equation adapted from Cunningham *et al.* (2019):

$$[\text{PE 545}] = \frac{\text{OD}_{\text{max}} + (\text{OD}_{\text{max}} \times p_{\text{sum}})}{\varepsilon \times d} \times \frac{V_{\text{b}}}{V_{\text{s}}} \times 10^3 \quad (2)$$

With  $\text{OD}_{\text{max}}$  the OD at the absorption peak;  $p_{\text{sum}}$  the proportion of cells remaining in the supernatant after culture centrifugation (7% for *T. amphioxeia*, 0% for *M. rubrum*);  $\varepsilon$  the mass extinction coefficient of PE 545:  $\varepsilon = 12.6 \text{ L.g}^{-1}.\text{cm}^{-1}$  (MacColl *et al.*, 1976);  $d$  the optical path length through the solution (0.579 cm);  $V_{\text{b}}$  the volume of phosphate buffer (4 mL);  $V_{\text{s}}$  the volume of culture sampled (10 mL). A molar mass  $\text{MW}_{\text{PE 545}} = 57.03 \text{ kDa}$

was used to convert the mass of PE 545 into moles (Protein Data Bank, code 1XF6, data from Doust *et al.*, 2004).

### Measurement of microalgae absorption

The coefficient of particulate absorption,  $a_{\text{p}}(\lambda)$ , was measured *in vivo* from 350 to 850 nm using a dual beam spectrophotometer equipped with a 150-mm integrating sphere (Perkin-Elmer, Lambda 1 050). Compared with other techniques (i.e. filter pad), measuring  $a_{\text{p}}(\lambda)$  on a suspension of living cells placed inside an integrating sphere was demonstrated as being the most accurate method (Röttgers and Gehnke, 2012; Stramski *et al.*, 2015). A 1 cm-width quartz cuvette containing a small volume of the culture was placed in the middle of the sphere using a white holder provided by the manufacturer. The coefficient of total absorption,  $a(\lambda)$ , was computed as:

$$a(\lambda) = \ln(10) \times \frac{\text{OD}_{\text{s}}(\lambda)}{d} \quad (3)$$

With  $\text{OD}_{\text{s}}$  the OD of the living cells suspended in the cuvette;  $d$  the optical path length in the cuvette (0.01 m). The absorption of the suspended particles was then computed by subtracting the contribution of pure seawater and of colored dissolved organic matter (CDOM), which was measured on the filtrate of culture samples filtered on a 0.2- $\mu\text{m}$  pore PES filter:

$$a_{\text{p}}(\lambda) = a(\lambda) - a_{\text{w}}(\lambda) - a_{\text{cdom}}(\lambda) \quad (4)$$

In the remaining of the present study,  $a_{\text{p}}(\lambda)$  will refer to *in vivo* particulate absorption measurements, unless specified otherwise. In order to compare with the filter pad method, the coefficient of particulate absorption was also measured on GF/F filters using the same spectrophotometer. The OD was measured on unfrozen GF/F filters, with the filter placed inside the integrating sphere. The coefficient of particulate absorption was computed in two steps. First, the absorption by particles was computed from OD without correction for pathlength amplification:

$$a_{\text{p}}^{\text{uncorr}}(\lambda) = \frac{\ln(10) \times \text{OD}_{\text{f}} \times A_{\text{f}}}{V} \quad (5)$$

With  $\text{OD}_{\text{f}}$  the OD measured on the filter;  $A_{\text{f}}$  the area of the colored zone on the filter and  $V$  the filtered volume. Second, the pathlength amplification was corrected individually for each sample using the *in vivo*  $a_{\text{p}}(\lambda)$  as the reference for true absorption, following an approach proposed by Röttgers and Gehnke (2012). Correcting for pathlength amplification is required when using the filter-pad technique because scattering in the particle/filter matrix lengthens the distance traveled by photons, thus significantly increasing OD measurements (Bricaud and Stramski, 1990). For comparison purposes, the coefficient of particulate absorption was also computed using a non-specific pathlength correction (Stramski *et al.*, 2015). Both methods for pathlength amplification correction are detailed in Supplementary Information 1. The contribution

of nonpigmented particles to  $a_p(\lambda)$  was not measured in the cultures.

### Calculation of absorption cross-section and pigment-specific absorption

The absorption cross-section,  $\sigma_a$ , in  $\text{m}^2 \cdot \text{cell}^{-1}$ , indicates the absorptive power of one algal cell (Stramski and Mobley, 1997). It was computed as:

$$\sigma_a(\lambda) = \frac{a_p(\lambda)}{N} \quad (6)$$

where  $N$  is the cell density of the sample (in  $\text{cells} \cdot \text{m}^{-3}$ );  $a_p(\lambda)$  is the coefficient of particulate absorption.

The pigment-specific absorption coefficient,  $a_p^*$ , in  $\text{m}^2 \cdot \text{mg}_{\text{pigment}}^{-1}$  indicates the efficiency of the absorption by pigments in the cells (Bricaud et al., 1995). Here, we focused on the pigment-specific absorption at 552 and 675 nm, which correspond to the maximum absorption wavelengths of PE 545 and chl *a*, respectively, and for which most of the absorption is due to that pigment:

$$a_p^*(675) = \frac{a_p(675)}{[\text{chl } a]} \quad (7a)$$

$$a_p^*(552) = \frac{a_p(552)}{[\text{PE } 545]} \quad (7b)$$

With  $a_p(\lambda)$  the particulate absorption at wavelength  $\lambda$  (in  $\text{m}^{-1}$ ); [pigment] the concentration of the pigment responsible for absorption at the same wavelength (in  $\text{mg} \cdot \text{m}^{-3}$ ). Additionally, the specific absorption coefficient of chl *a* at 665 nm  $a_p^*(665)$  was calculated and used for the analysis of field and satellite radiometric measurements.

## MESODINIUM RUBRUM BLOOM OBSERVATIONS

### Field sampling

*In situ* samples were collected at eight stations during a *M. rubrum* bloom off the French Atlantic coast on 29 March 2021 (Fig. 1E–G). Water samples were collected at the surface using a bucket, gently stirred to homogenize phytoplankton concentration, and poured into 2-L bottles. Bottles were conserved in the dark at ambient temperature until subsequent laboratory analyses, within 2–4 hours after sampling. Back in the laboratory, the samples were filtered on GF/F filters and stored at  $-80^\circ\text{C}$  until pigments analysis by HPLC. The particulate absorption coefficient was measured on filters as described earlier. Pathlength amplification was corrected with the two methods mentioned previously and detailed in [Supplementary Information 1](#). To better compare with microalgae culture, the particulate absorption coefficient measured on *in situ* samples was further partitioned into absorption by phytoplankton,  $a_{\text{phy}}(\lambda)$ , and by nonpigmented particles, using bleach for pigment extraction (Roesler et al., 2018).

Above-water radiometric measurements were performed concomitantly to water sampling. The upwelling radiance,  $L_u(\lambda)$ ;

downwelling radiance,  $L_d(\lambda)$ ; and sky radiance,  $L_{\text{sky}}(\lambda)$ , were sequentially measured following a standard protocol (Mueller, 2003) using a hand-held spectroradiometer (ASD Fieldspec, HandHeld 2). The air–water interface reflection coefficient of the sky radiance,  $\rho$ , was calculated as a function of wind speed, sea state, sky conditions and geometry of acquisition at the time of field measurement (Ruddick et al., 2006). The remote sensing reflectance,  $R_{\text{rs}}(\lambda)$ , was computed as:

$$R_{\text{rs}}(\lambda) = \frac{L_u(\lambda) - \rho L_{\text{sky}}(\lambda)}{\pi L_d(\lambda)} \quad (8)$$

### Satellite data acquisition and processing

On-board Sentinel-2 (S2), the multi-spectral imager (MSI) makes it possible to observe phytoplankton coastal blooms at high spatial resolution (Caballero et al., 2020). Here, two S2 images were available during the *M. rubrum* red tide on the 27 and 29 March 2021 (Fig. 1F–G) and used to map chl *a* concentration ([chl *a*]). Top-of-atmosphere Level-1C products were downloaded from the Copernicus open access hub (<https://dataspace.copernicus.eu/>) and resampled at 20 m. The GRS algorithm for atmospheric correction and sunglint removal (Harmel et al., 2018) was applied to L1C data to retrieve the bottom-of-atmosphere spectral remote-sensing reflectance,  $R_{\text{rs}}(\lambda)$ . The GRS atmospheric correction was previously validated during high biomass phytoplankton blooms, including red tides of *M. rubrum* (Gernez et al., 2023).

For each pixel, chl *a* was computed from  $R_{\text{rs}}(\lambda)$  using a semi-analytical red-edge algorithm (Gons, 1999; Gons et al., 2002) recalibrated for S2/MSI (Gernez et al., 2017). This algorithm is based on the common radiative transfer approximation (Morel and Prieur, 1977):

$$R_{\text{rs}}(\lambda) \sim \frac{b_b(\lambda)}{b_b(\lambda) + a(\lambda)} \quad (9)$$

The backscattering coefficient,  $b_b$ , is computed from  $R_{\text{rs}}(\lambda)$  at 783 nm using the assumption that in the near-infrared spectral range, the absorption coefficient is dominated by pure seawater:

$$b_b = \frac{1.56 \pi R_{\text{rs}}(783)}{0.082 - 0.6 \pi R_{\text{rs}}(783)} \quad (10)$$

Then,  $a_{\text{phy}}(665)$  is retrieved from the red-edge band ratio  $R_{\text{rs}}(705)/R_{\text{rs}}(665)$ , assuming that  $b_b$  is spectrally neutral from 665 to 783 nm, and that at 665 and 705 nm, the absorption coefficient by nonalgal particles and CDOM is negligible compared with that of chl *a* and pure seawater:

$$a_{\text{phy}}(665) = (0.7 + b_b) \frac{R_{\text{rs}}(705)}{R_{\text{rs}}(665)} - 0.4 - b_b^p \quad (11)$$

The tuning parameter,  $p$ , was set to 1.02 (Gernez et al., 2017).

Finally, the chl *a* concentration is computed from  $a_{\text{phy}}(665)$  using:

$$[\text{chl } a] = \frac{a_{\text{phy}}(665)}{a_{\text{phy}}^*(665)} \quad (12)$$

With  $a_{\text{phy}}^*(665)$  the chl *a* specific absorption coefficient at 665 nm. In the initial version of the algorithm,  $a_{\text{phy}}^*(665)$  was calibrated using a variety of *in situ* measurements performed in inland and coastal waters (Gons *et al.*, 2002). Here,  $a_{\text{phy}}^*(665)$  was estimated from field measurements performed during the bloom of *M. rubrum*. In practice,  $a_{\text{phy}}^*(665)$  was determined as the slope of a linear fit between  $a_{\text{phy}}(665)$  and chl *a* concentration, with  $a_{\text{phy}}(665)$  retrieved from the *in situ*  $R_{\text{rs}}(\lambda)$  measurements using equations (8–11). Finally, the fitted  $a_{\text{phy}}^*(665)$  was compared with the range of bio-optical variability measured during the laboratory photoacclimation experiment.

### Data analysis

Preliminary analysis of flow cytometry data was computed with the software MACSQuantify™ version 2.13.0 (Miltenyi Biotech). For the photoacclimation experiments, data analyses were performed with the R software, version 4.2.2 (R Core Team, 2022), with packages from the tidyverse project (Wickham *et al.*, 2019), and packages cmocean (Thyng *et al.*, 2016), ggpubr (Kassambara, 2023), reshape2 (Wickham, 2007) and viridis (Garnier *et al.*, 2023). With the exception of the atmospheric correction, the processing of satellite S2 data was performed using the Sentinel application platform (SNAP) software of the European Space Agency (ESA), version 9.0.0.

## RESULTS

### Photoacclimation experiment

#### *Different growth rates but similar light saturation in M. rubrum and T. amphioxeia*

*Mesodinium rubrum* and *T. amphioxeia* were able to grow in culture over the investigated range of irradiance. For both species, growth rate was minimal at the lowest irradiance (20  $\mu\text{mol photons.m}^{-2}.\text{s}^{-1}$ ) and maximal at the highest irradiance (200 or 220  $\mu\text{mol photons.m}^{-2}.\text{s}^{-1}$ ). A fit with a Poisson function gives an estimate of the maximum growth rate ( $\mu_{\text{m}}$ ) and of the light saturation parameter for growth ( $K_{\text{E}}$ ) which delimits the boundary between growth-limiting and growth-saturating irradiances (Fig. 2A). *Teleaulax amphioxeia* grew much faster than *M. rubrum* ( $\mu_{\text{m}} = 0.94 \pm 0.04 \text{ d}^{-1}$  in *T. amphioxeia* versus  $0.47 \pm 0.04 \text{ d}^{-1}$  and  $0.32 \pm 0.01 \text{ d}^{-1}$  in *M. rubrum* at 21 and 17.5°C, respectively) but showed similar  $K_{\text{E}}$ , suggesting similar adaptation to irradiance, although the precision of  $K_{\text{E}}$  estimation can be subject to caution regarding the few irradiance levels (3 to 4) used to fit the model. In terms of volume, *M. rubrum* cells were about 100 times bigger than *T. amphioxeia* cells (Fig. 2B). Both cultures exhibited differences in cell biovolume, depending on irradiance and temperature. In particular, *M. rubrum* cells were smaller at low irradiances compared with 120 or 220  $\mu\text{mol photons.m}^{-2}.\text{s}^{-1}$ , and generally smaller at 21°C compared with 17.5°C.

#### *Mesodinium rubrum photoacclimated pigment phenotypes are similar to those of its cryptophyte prey*

The analysis of lipophilic pigments by HPLC revealed the presence of the same pigments in both species, namely chl *a*, chl *c*<sub>2</sub>, alloxanthin,  $\beta,\epsilon$ -carotene, crocoxanthin and monadoxanthin, which are the typical lipophilic pigments of cryptophyte plastids (Figs 3 and S2). Minimal concentrations of pheopigments were detected in some cultures: pheophorbide *a* in *M. rubrum* cultures at 120 and 220  $\mu\text{mol photons.m}^{-2}.\text{s}^{-1}$ ; and pheophytin *a* in the same cultures and in all cultures of *T. amphioxeia* (Fig. S2). This indicates the degradation of chl *a* in these cultures, possibly due to the death of some cells. In the aqueous extracts of cultures, a single absorption peak at 552 nm with a shoulder at 565 nm was observed (Fig. S3A). This seems to confirm the presence of PE 545 as the only PBP in both species, though the maximum absorption wavelength showed a 7-nm offset. The slight offset between the observed (552 nm) *vs.* expected (545 nm) wavelength of the PE absorption maximum might result from a photoacclimation process occurring at the molecular level, in response to the spectral shape of the light field used to illuminate the cultures (Spangler *et al.*, 2022).

Pigment concentrations per cell biovolume were higher in *T. amphioxeia* than in *M. rubrum* at all irradiance levels, for chl *a*, chl *c*<sub>2</sub>, alloxanthin and PE 545 (Fig. 3), consistent with the observed important space occupied by the chloroplast in the minute cell of *T. amphioxeia*, compared with the ciliate (Fig. 1B and D). Chl *a*, chl *c*<sub>2</sub> and alloxanthin concentrations decreased with irradiance in both species (Fig. 3A–C). PE 545 cellular concentration showed a sharp decrease between 20 and 200  $\mu\text{mol photons.m}^{-2}.\text{s}^{-1}$  in both species at 21°C (4.5-fold decrease for *T. amphioxeia* and 3-fold decrease for *M. rubrum*). For *M. rubrum* at 17.5°C however, only a small decrease at 220  $\mu\text{mol photons.m}^{-2}.\text{s}^{-1}$  was observed (Fig. 3D). It is important to note that *M. rubrum* cultures at 17.5°C were sampled after a short period of photoacclimation (5 days), that corresponds to 1 to 2 generations given the observed growth rates. While the differences in pigment content between irradiance levels are already apparent, the cells in these cultures were still in the process of photoacclimation, and are not representative of fully acclimated phenotypes.

#### *Absorption properties of M. rubrum and T. amphioxeia show classical photoacclimation responses*

The absorption spectra of both species were almost identical in shape, consistent with the fact that the exact same pigments were identified in *M. rubrum* and *T. amphioxeia* (Fig. S4). For both species, the spectral shape of the absorption coefficient was consistent with the presence of chl *a*, chl *c*<sub>2</sub>, alloxanthin, and PE 545, with respective absorption peaks at 443 and 675, 460, 460 and 490, and 552 nm. The spectral signature of PE was only clearly visible when the absorption was measured from a suspension of living cells. When measured using the filter-pad technique, the absorption spectra lacked the characteristic peak of PE 545 (Fig. 4).

Cell absorption cross-section at 675 nm decreased sharply between 20 and 80  $\mu\text{mol photons.m}^{-2}.\text{s}^{-1}$  in *T. amphioxeia* (–24%) and *M. rubrum* (–42%), followed by a much slighter decrease between 80 and 200  $\mu\text{mol photons.m}^{-2}.\text{s}^{-1}$  (Fig. 5A).

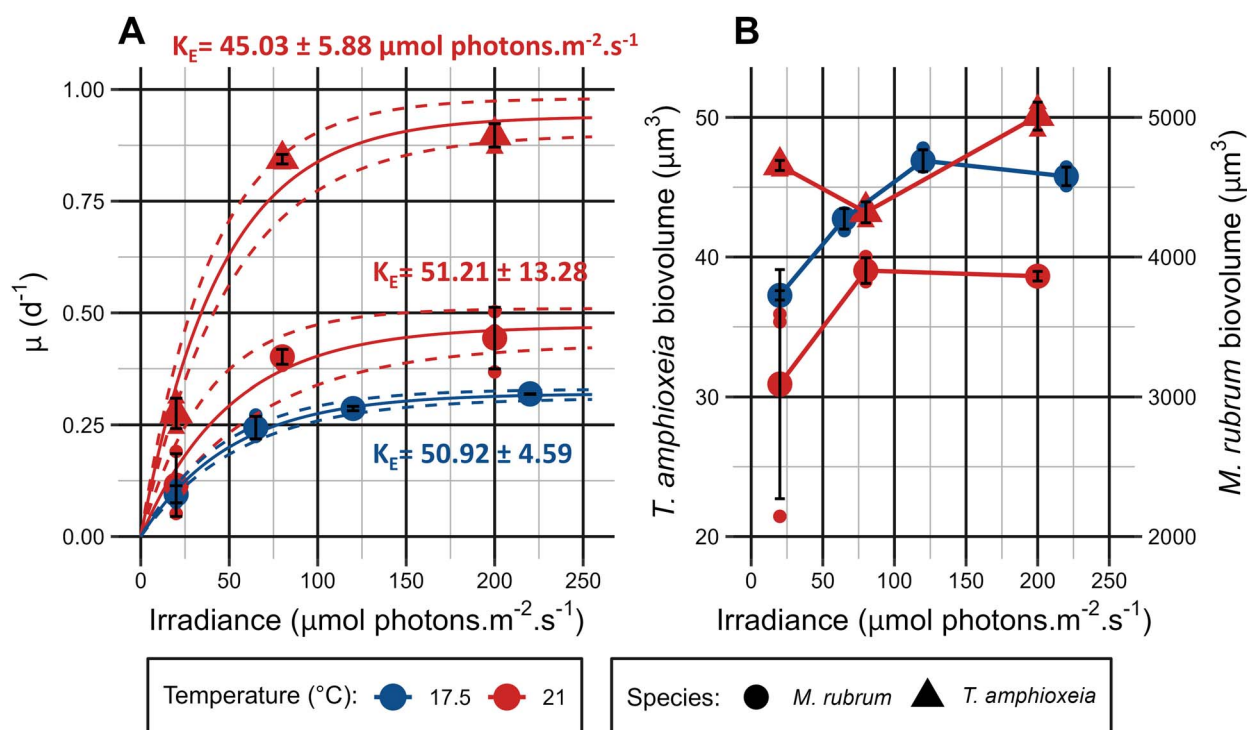


**Fig. 2.** (A) Growth rate as a function of irradiance for *T. amphioxeia* (triangles) and *M. rubrum* (circles), at 17.5°C (blue) and 21°C (red). Growth curves result from an exponential Poisson model (Eq. 1) fitted on the data.  $K_E \pm$  standard error is indicated for each growth curve. (B) Cell biovolume (ESD) of *T. amphioxeia* and *M. rubrum* as a function of irradiance. Smaller symbols: individual replicates, bigger symbols: mean of three replicates, error bars: standard deviation.

The chl *a*-specific absorption coefficient at 675 nm increased between the minimal and maximal irradiance levels, by 27% for *T. amphioxeia* and by 17% for *M. rubrum* (Fig. 5B). All values of  $a_p^*(675)$  measured on cultures remained below the theoretical limit of absorption by chl *a* in seawater,  $a_{sol,chl a}^*(675) = 0.0334$  (Bricaud et al., 2004), indicating some packaging effect in pigment absorption. For *T. amphioxeia*,  $a_p^*(675)$  was higher than for *M. rubrum*, showing that the packaging effect was lower in the cryptophyte than in the ciliate. This is coherent with the theory of Morel and Bricaud (1981), which predicts that packaging effect is proportional to the size of the phytoplankton cell.

For both species at 21°C, absorption properties at 552 nm showed similar trends to those at 675 nm.  $\sigma_a(552)$  displayed a 48 and 62% decrease from 20 to 80  $\mu\text{mol photons.m}^{-2}.\text{s}^{-1}$  in *M. rubrum* and *T. amphioxeia*, respectively, followed by a slighter decrease between 80 and 200  $\mu\text{mol photons.m}^{-2}.\text{s}^{-1}$  in both species (Fig. 5C). Between 20 and 200  $\mu\text{mol photons.m}^{-2}.\text{s}^{-1}$ , the phycoerythrin-specific absorption coefficient increased by 57% in *T. amphioxeia*.  $a_p^*(552)$  was lower in *M. rubrum*, with similar values at 20 and 80  $\mu\text{mol photons.m}^{-2}.\text{s}^{-1}$ , and a 27% increase at the highest irradiance level (Fig. 5D).

### Comparison with field measurements and satellite remote sensing

#### *Mesodinium rubrum* pigment composition in laboratory, field and literature data

We compared the accessory pigment/chl *a* ratios observed in our experiments with the results from a previous study (Rial et al., 2013) in which *M. rubrum* was cultured at 2 irradiance

levels (70 and 200  $\mu\text{mol photons.m}^{-2}.\text{s}^{-1}$ ). Overall, chl *c*<sub>2</sub>/chl *a*, alloxanthin/chl *a* and  $\beta,\epsilon$ -carotene/chl *a* ratios were comparable in both studies, though some differences emerge (Fig. 6). Rial et al. (2013) observed an increase of the chl *c*<sub>2</sub>/chl *a* ratio at high light compared with low light, no clear increase of the alloxanthin/chl *a* ratio with irradiance and a  $\beta,\epsilon$ -carotene/chl *a* ratio lower than in the present study. The results from the culture were also compared with that of field samples acquired during a bloom of *M. rubrum* in Venezuela (Guzmán et al., 2016) or in France (this study). Pigment/chl *a* ratios were very similar in both sampling locations. *In situ* samples showed chl *c*<sub>2</sub>/chl *a* and  $\beta,\epsilon$ -carotene/chl *a* ratios comparable to what was observed in cultures, but the alloxanthin/chl *a* ratio was markedly lower (Fig. 6), certainly because of the contribution of other phytoplankton taxa to the chl *a* biomass in natural environments. In samples from the 2021 *M. rubrum* bloom in France, pigments not specific to cryptophyte plastids were detected, namely fucoxanthin, peridinin and diadinoxanthin. This indicates that the bloom was not strictly monospecific, although largely dominated by *M. rubrum*. In particular, cells of the dinoflagellate *Scrippsiella sp.* were identified in preserved samples (Anne Schmitt, IFREMER LERMPL, Nantes, personal communication).

#### Optical characteristics and satellite remote sensing of a *M. rubrum* bloom

The particulate absorption coefficients measured *in vivo* (i.e. on suspended cells) was used as a reference to correct for path-length amplification on filter pad measurements of corresponding cultures (Röttgers and Gehnke, 2012). It was compared with

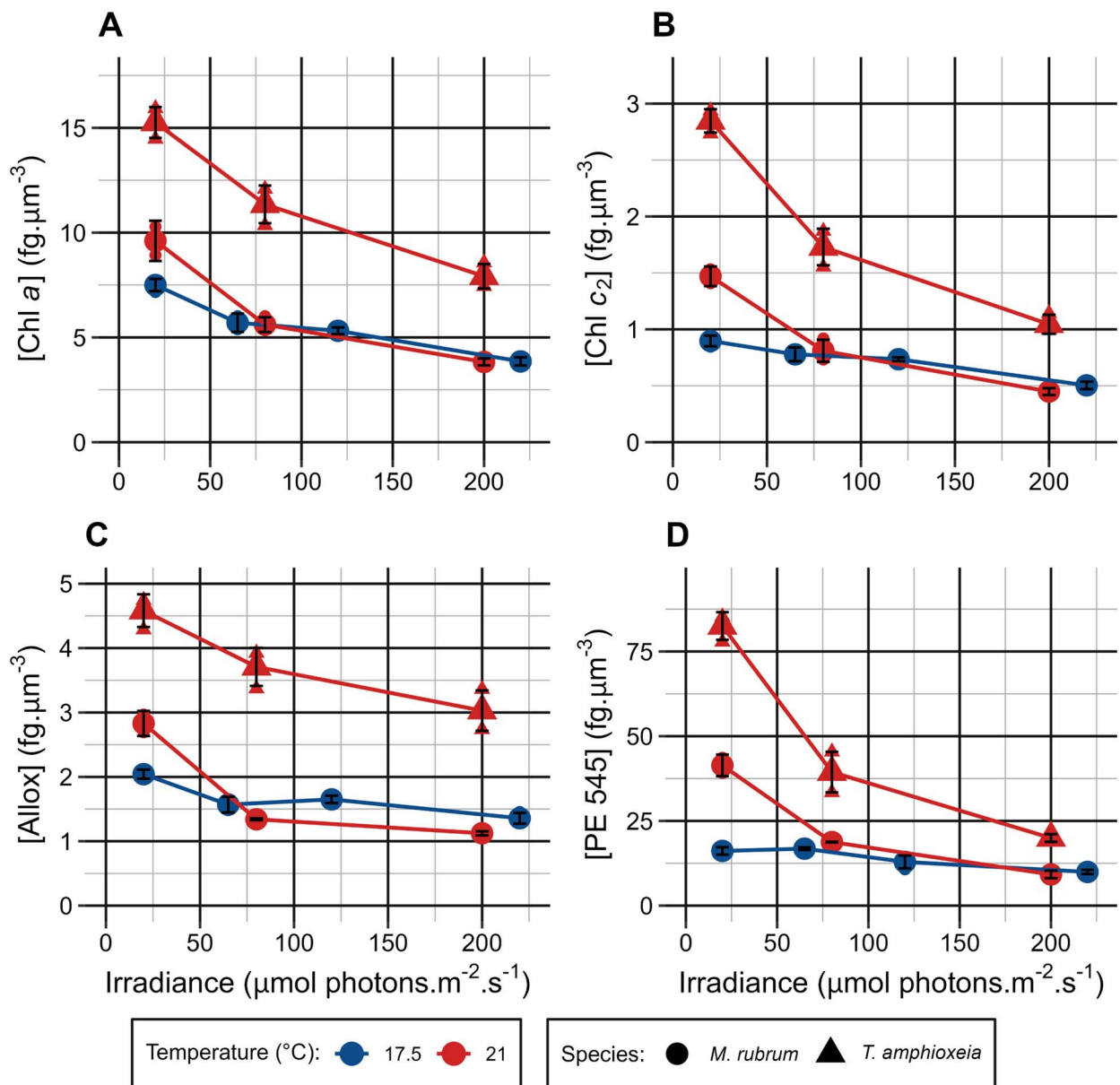


**Fig. 3.** Concentrations of different pigments per biovolume (A: chl *a*, B: chl *c*<sub>2</sub>, C: alloxanthin and D: PE 545) as a function of irradiance, in *T. amphioxeia* (triangles) and *M. rubrum* (circles), at 17.5°C (blue) and 21°C (red). Note that photoacclimation time differs between temperature conditions: 5 days for 17.5°C and 12–13 days for 21°C. Smaller symbols: individual replicates, bigger symbols: mean of three replicates, error bars: standard deviation.

$a_p(\lambda)$  obtained using a generic correction proposed by Stramski *et al.* (2015) (Suppl. Info. 1 and Fig. S5A). In the specific case of *M. rubrum* culture samples, the standard correction seems to overestimate  $a_p(\lambda)$ , with discrepancies increasing with the magnitude of absorption. However, when applied to the much lower absorption values from the bloom, the two corrections gave similar results. Compared with values of modeled  $a_{\text{phy}}(665)$  obtained from the inversion of *in situ* reflectance,  $a_{\text{phy}}(665)$  values measured with the filter pad technique are generally higher (more than twice higher for certain stations) regardless of which correction is applied. A linear regression of  $a_{\text{phy}}(665)$  against the corresponding *in situ* [chl *a*] measured at each station led to several estimates of  $a_{\text{phy}}^*(665)$  in the *M. rubrum* bloom (Fig. S5B),

with important discrepancies between the two methods (i.e. filter pad measurement or reflectance inversion) used for evaluating microalgal absorption in the bloom.

The linear regression of modeled  $a_{\text{phy}}(665)$  versus [chl *a*] gives an estimated  $a_{\text{phy}}^*(665)$  in the *M. rubrum* bloom of  $0.0144 \text{ m}^2 \cdot \text{mg}_{\text{chl } a}^{-1}$  (adjusted  $R^2 = 0.9046$ ,  $P$ -value  $< 0.001$ ). This value is very close to the  $a_{\text{phy}}^*(665) = 0.0146 \text{ m}^2 \cdot \text{mg}_{\text{chl } a}^{-1}$  determined by Gons *et al.* (2002) for a range of phytoplankton communities in coastal ecosystems. In contrast, using  $a_{\text{phy}}(665)$  measured on filters leads to high estimations of  $a_{\text{phy}}^*(665)$ , close to or past the theoretical limit of the specific absorption coefficient of chl *a* in seawater at 665 nm ( $0.0217 \text{ m}^2 \cdot \text{mg}^{-1}$ , Bricaud *et al.*, 2004). The potential reasons for this mismatch are

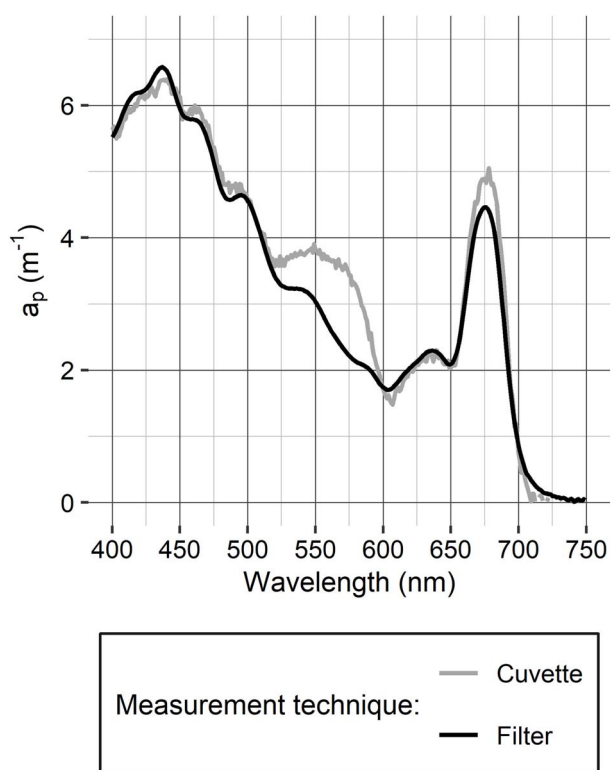


**Fig. 4.** Absorption spectra of a *M. rubrum* culture (irradiance  $80 \mu\text{mol photons}\cdot\text{m}^{-2}\cdot\text{s}^{-1}$ , mean of all replicates) measured on living cells suspended in water (gray); and using the filter-pad technique (black), with a correction for pathlength amplification.

discussed further in this article. The value of  $a_{\text{phy}}^*(665)$  determined from modeled  $a_{\text{phy}}(665)$  was preferred for subsequent analyses, because it was closer to the values measured in the photoacclimation experiment and to the coefficient provided by Gons et al. (2002).

The values of  $a_{\text{phy}}^*(665)$  for *M. rubrum* observed in this study range from  $0.0071 \text{ m}^2\cdot\text{mg}_{\text{chl } a}^{-1}$  (lowest value observed in culture) to  $0.0144 \text{ m}^2\cdot\text{mg}_{\text{chl } a}^{-1}$  (field measurements from the bloom) (Fig. 7A). The  $a_{\text{phy}}^*(665)$  observed in the field is substantially higher than the highest measured in cultures of *M. rubrum* ( $0.0111 \text{ m}^2\cdot\text{mg}_{\text{chl } a}^{-1}$ ). All these values are below the specific absorption coefficient of chl *a* in seawater, indicating some degree of package effect of chl *a* in *M. rubrum*. The sensitivity of the chl *a*-retrieval algorithm of Gons et al. (2002) to the choice of  $a_{\text{phy}}^*(665)$  was illustrated by plotting [chl *a*] as a function of  $a_{\text{phy}}^*(665)$ , for three different values of  $a_{\text{phy}}(665)$  observed in the S2 image on 2021/03/27 (Fig. 7B). The values of  $a_{\text{phy}}^*(665)$  represented in Fig. 7A are plotted as vertical lines, to illustrate the influence of the choice of one specific value of  $a_{\text{phy}}^*(665)$  on the calculation of [chl *a*]. The percentage of variation of [chl *a*] depending on  $a_{\text{phy}}^*(665)$  is independent of  $a_{\text{phy}}(665)$ , but as [chl *a*] decreases exponentially when  $a_{\text{phy}}^*(665)$  increases, the absolute variability is more important for higher values of  $a_{\text{phy}}(665)$  (Supplementary table 1). This means that the uncertainty in remotely assessed [chl *a*] induced by different  $a_{\text{phy}}^*(665)$  is maximized in the case of concentrated patches of microalgal blooms.

The value of  $a_{\text{phy}}^*(665)$  determined *in situ* from the bloom samples was implemented into the algorithm of Gons et al. (2002) to create a map of [chl *a*] from the two Sentinel-2 images of the *M. rubrum* bloom on March 27 and 29, 2021 (Fig. 8). On March 27, [chl *a*] reached  $250 \text{ mg}\cdot\text{m}^{-3}$  in the most concentrated patches of the bloom. The distribution of chl *a* in the area was highly heterogeneous, with concentrated patches of [chl *a*]  $> 100 \text{ mg}\cdot\text{m}^{-3}$  forming narrow, filament-like structures  $\sim 50\text{--}150 \text{ m}$  wide and  $1.5\text{--}3 \text{ km}$  long, surrounded by less-concentrated areas with [chl *a*]  $< 5 \text{ mg}\cdot\text{m}^{-3}$  (Fig. 8A). On March 29, [chl *a*] was markedly lower throughout the area, with maxima around  $40 \text{ mg}\cdot\text{m}^{-3}$ . The spatial extent of the bloom was visibly reduced compared with the previous image, with most patches close to the coastline (Fig. 8B).

## DISCUSSION

### Biological and ecological implications of photoacclimation in *M. rubrum* and *T. amphioxeia*

Photoacclimation of pigment content in phytoplankton is a classic response to changes in irradiance, by which the rate of light absorption is fine-tuned to the energy needs of the cell (MacIntyre et al., 2002). Modification of chl *a* content has been described in polar strains of *M. rubrum* (Johnson and Stoecker, 2005; Moeller et al., 2011; Johnson et al., 2023), but the response of the other pigments has largely been overlooked. To our knowledge, the only study that mentions the photoacclimation of phycoerythrin cellular content in this ciliate is that of Moeller et al. (2011). Our results show that temperate strains of *M. rubrum* also have the ability to photoacclimate. Moreover, we observed that *M. rubrum* and *T. amphioxeia* pigment phenotypes display similar photoacclimation responses, where increasing irradiance is correlated with a decrease in the cellular content of all photosynthetic pigments (Fig. 3, Fig. S2). More specifically, the PE 545/chl *a* ratio shows a sharp decrease with increasing irradiance in both species (Fig. S6). This highlights the role of phycoerythrins in low-light environments in cryptophytes (Mendes et al., 2023) and in their ciliate predator. Nevertheless, *M. rubrum* and its prey display differences in the mechanisms involved in photoacclimation. The most striking one is that photoacclimation in the cryptophytes *Teleaulax* and *Geminigera* is mediated by finely regulating the transcription of nucleus-encoded genes, while this light-dependent regulation is absent in the kleptokaryon of *M. rubrum* (Altenburger et al., 2021; Johnson et al., 2023). Given that the pigment phenotype of *M. rubrum* acclimates to changing light conditions, post-transcriptional processes are necessarily involved in the regulation of pigment synthesis, for both lipophilic pigments and PBP. The evolutionary selection of such processes needed for photoacclimation in the ciliate can lead to two observations. First, it indicates that *M. rubrum* has reached a degree of specialization toward photosynthesis that seems unparalleled in other mixotrophic ciliates (Johnson et al., 2023), and therefore occupies a peculiar trophic position among them as both a voracious (albeit specific) predator of nanophytoplankton and a significant contributor to primary production (Yih et al., 2004; Johnson et al., 2013). Second, it suggests that the ability to photoacclimate constitutes an important evolutionary bottleneck for planktonic organisms

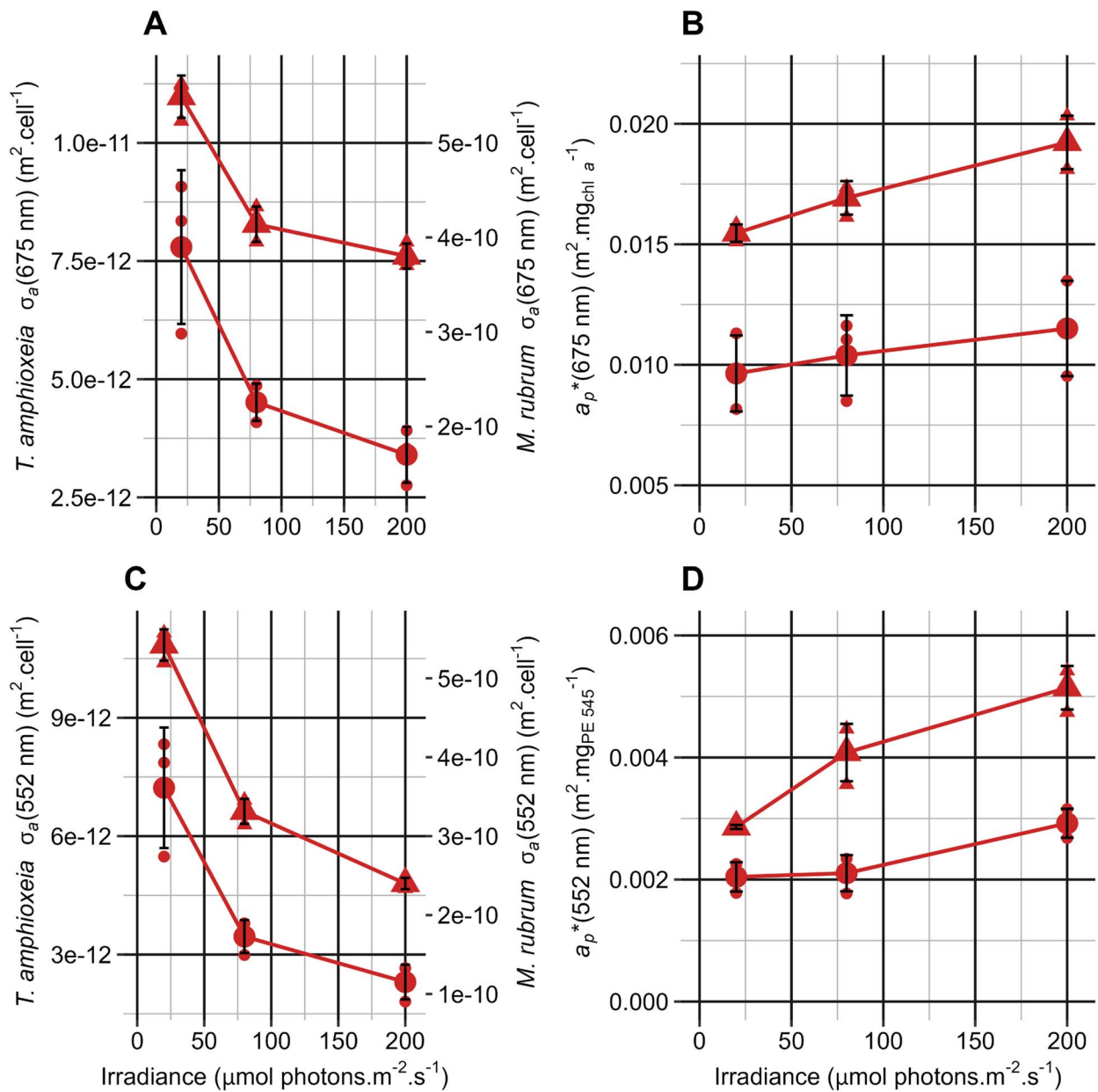


**Fig. 5.** Optical properties of *T. amphioxeia* (triangles) and *M. rubrum* (circles), at 21°C, calculated using the *in vivo* absorption. (A) Cell absorption cross section at 675 nm. (B) chl *a*-specific absorption coefficient at 675 nm. (C) Cell absorption cross-section at 552 nm. (D) PE 545-specific absorption coefficient at 552 nm. Smaller symbols: individual replicates, bigger symbols: mean of three replicates, error bars: standard deviation.

that rely on photosynthesis as their main trophic strategy, occurring in the early steps of permanent plastid acquisition. Six *et al.* (2021) demonstrated the key role that photosynthesis regulation and photoprotection play in the adaptation to cold or warm waters in marine cyanobacteria. The occurrence of *M. rubrum* across a wide range of latitudes (Dolan and Marrasé, 1995; van den Hoff and Bell, 2015) begs the question of the physiological and molecular adaptations of different strains to their respective environments, and of possible differences in photoacclimation responses between those strains. We should also note that ‘behavioral’ adaptations, in association with photosynthesis regulation, probably play a significant role in

the photophysiology of *M. rubrum*. Indeed, this highly motile organism seems to display irradiance-dependent phototaxis (Fenchel and Hansen, 2006) and performs important diel vertical migrations (Smith Jr. and Barber, 1979; Crawford, 1989). To what extent these migrations constitute an adaptation that maximizes photosynthetic growth and/or limits grazing pressure by predators remains in question.

One interesting aspect that our experiment did not control for is the importance of prey plastid photoacclimation for predator photophysiology, as the ciliates at all irradiance levels were fed with prey acclimated to low light ( $20 \mu\text{mol photons.m}^{-2}.\text{s}^{-1}$ ). Considering the pigment concentrations in

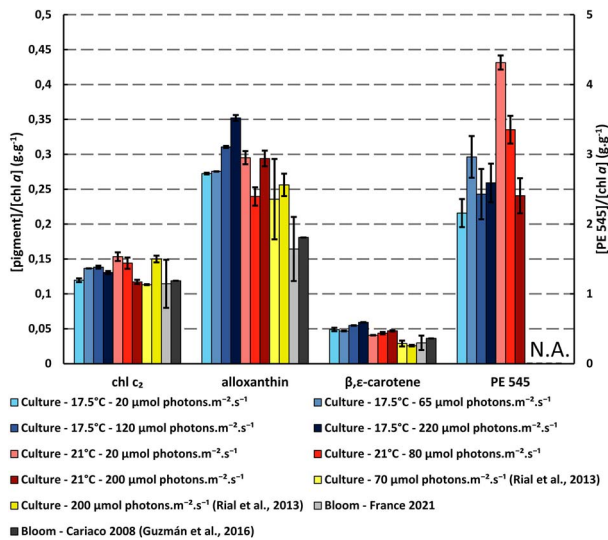


**Fig. 6.** Comparison of  $[\text{pigment}]/[\text{chl } a]$  ratios for different *M. rubrum* cultures (this study; Rial et al., 2013), and pigment samples from *M. rubrum* blooms (French Atlantic coast, 2021, this study; Cariaco Basin, 2008, Guzmán et al., 2016). Bar height shows the mean of all replicates, and error bars show the standard deviation when available. N.A. = no data available (pigment concentration not measured).

high light-acclimated *M. rubrum* ( $200 \mu\text{mol photons}\cdot\text{m}^{-2}\cdot\text{s}^{-1}$ ) and low light-acclimated *T. amphioxeia*, *M. rubrum* growth rate and the ingestion rate of *T. amphioxeia* cells by *M. rubrum*, we calculated that ingested prey pigments could contribute up to 22% of the total pigment content of *M. rubrum* (Suppl. Info. 2). While this is certainly a significant contribution, it means that the vast majority ( $>78\%$ ) of the pigments are still directly produced *de novo* by *M. rubrum* cells, and that the observed photoacclimated phenotypes result mainly from ciliate metabolism. It is also worth noting that low light-acclimated cryptophytes that were added to high light environments likely experienced photooxidative stress, that the ciliate experienced as well after prey ingestion. This probably exerted an influence on the ciliate's physiology that we did not account for, but nevertheless highlights interesting questions regarding the importance of prey plastid photoacclimation in kleptoplastidic protists.

### Variability of optical properties in *M. rubrum* cultures and blooms

Besides its implications in *M. rubrum* biology and ecology, photoacclimation can also play a role in the variability of seawater optical properties. It is widely recognized that phytoplankton are among the main drivers of optical variability in the surface ocean, with phytoplankton optical properties being influenced by changes in phytoplankton composition as well as by changes in the optical properties of individual cells of any species (Stramski et al., 2001, 2002). In the case of massive blooms dominated by a single species, such as in *M. rubrum* red tides, optical variability primarily results from changes in the optical properties of individual cells of the dominant species. Here, we focused on changes in absorption cross-section and chl *a*-specific absorption and how it can potentially

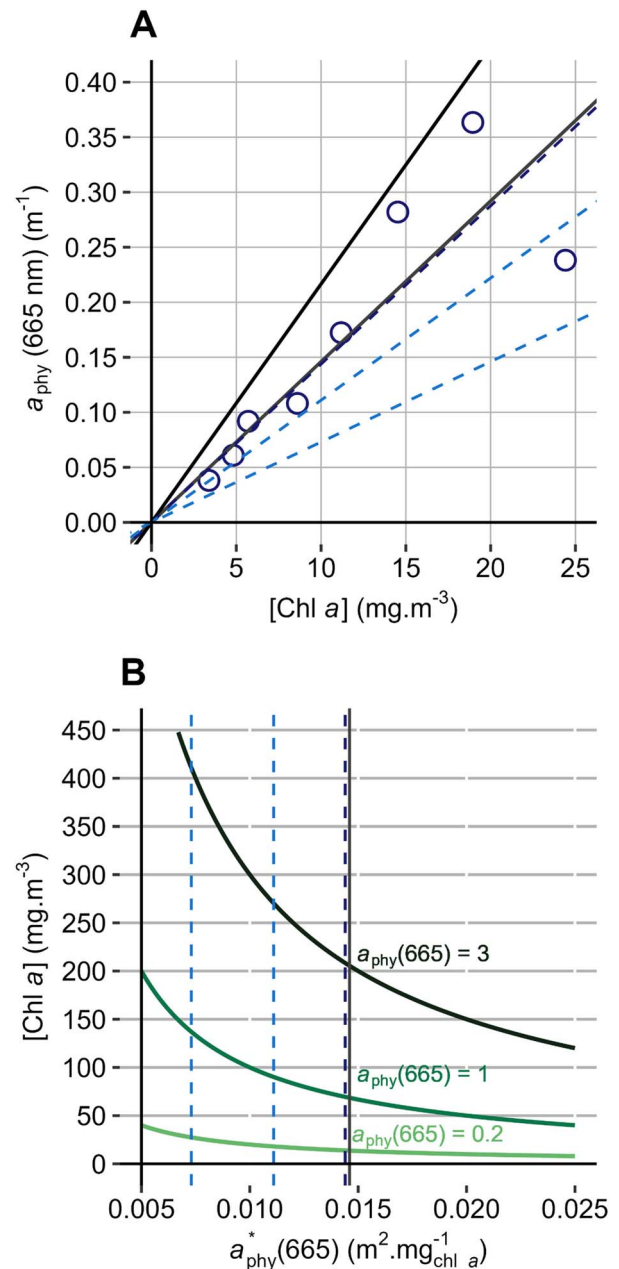


**Fig. 7.** (A) Chl *a* concentrations vs *in situ*  $a_{\text{phy}}(665)$  derived from the above-water remote-sensing reflectance (inversion algorithm of Gons et al., 2002): the blue circles represent the values for the eight stations in the bloom. Lines represent different values of  $a_{\text{phy}}^*(665)$ : solid black: upper theoretical limit for  $a_{\text{phy}}^*(665) = 0.0217 \text{ m}^2\cdot\text{mg}_{\text{chl } a}^{-1}$  (Bricaud et al., 2004); solid gray: average value of  $a_{\text{phy}}^*(665) = 0.0146 \text{ m}^2\cdot\text{mg}_{\text{chl } a}^{-1}$  determined by Gons et al. (2002) for a range of coastal ecosystems; dashed dark blue: linear regression on the correspondence of modeled  $a_{\text{phy}}(665)$  and measured  $[\text{chl } a]$ ,  $a_{\text{phy}}^*(665) = 0.0144 \text{ m}^2\cdot\text{mg}_{\text{chl } a}^{-1}$ ; dashed light blue: upper ( $a_{\text{phy}}^*(665) = 0.0111 \text{ m}^2\cdot\text{mg}_{\text{chl } a}^{-1}$ ) and lower ( $a_{\text{phy}}^*(665) = 0.0071 \text{ m}^2\cdot\text{mg}_{\text{chl } a}^{-1}$ ) values of  $a_{\text{phy}}^*(665)$  from the *M. rubrum* photoacclimation experiment (this study). (B)  $[\text{chl } a]$  as a function of  $a_{\text{phy}}^*(665)$ , for three different values of  $a_{\text{phy}}(665)$  (in  $\text{m}^{-1}$ ). Vertical lines represent values of  $a_{\text{phy}}^*(665)$  as presented in A (upper and lower experimental values in dashed blue; *in situ* value in dashed dark blue; Gons et al., 2002 in solid gray).

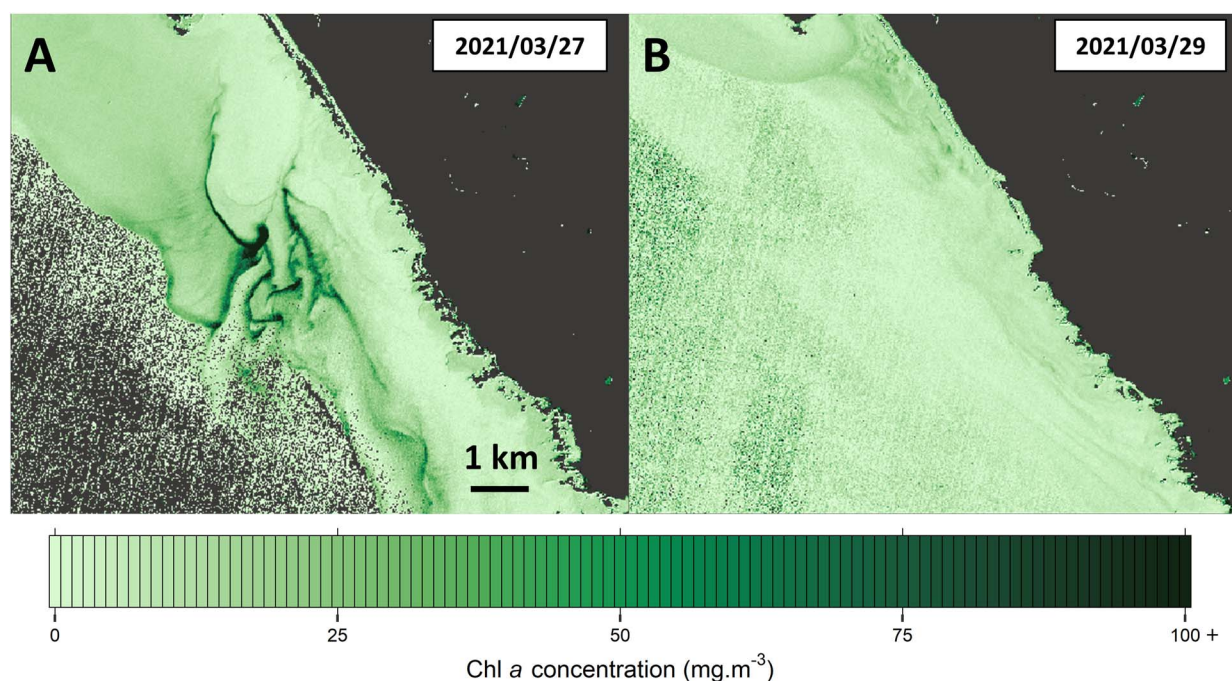


**Fig. 8.** Maps of chl *a* concentration (in  $\text{mg}\cdot\text{m}^{-3}$ ) in the *M. rubrum* bloom off the coast of France, in March 2021. Sentinel-2 satellite images are the same as in Fig. 1. [Chl *a*] is derived from satellite remote-sensing reflectance using the inversion algorithm of Gons *et al.* (2002), with  $a_{\text{phy}}^*(665) = 0.0144 \text{ m}^2\cdot\text{mg}\cdot\text{chl } a^{-1}$  (A) 27 March 2021, (B) 29 March 2021. Land and glint-contaminated pixels have been flagged and are colored in dark gray.

influence estimation of [chl *a*] using satellite remote sensing (see Remote sensing of *M. rubrum* blooms).

In *T. amphioxeia* and *M. rubrum*, cell absorption cross-section was maximal at the lowest irradiance and minimal at the highest, while pigment-specific absorption coefficients (for both chl *a* and PE 545) followed an opposite trend (Fig. 5), a classical response for these parameters (MacIntyre *et al.*, 2002). We observe in particular that the *in vivo* absorption associated with PE 545 at 552 nm follows the same irradiance-dependent pattern as the absorption associated with chl *a* at 675 nm. This indicates that cryptophyte PBPs, although different in structure and localization from other photosynthetic pigments (including cyanobacterial and rhodophytan PBPs), are submitted to similar bio-optical constraints, such as packaging effect.

The field measurements presented in this study show that the chl *a*-specific absorption of *M. rubrum* in the bloom is higher than that of cultures even at the highest irradiance, indicating a “high light-acclimated” phenotype. This may be explained in part by the aggregation of *M. rubrum* in a thin layer near the surface, in an environment saturated with light (as observed and reviewed by Crawford, 1989). Moreover, phytoplankton phenotypes observed in the environment are generally less pigmented than their cultured counterparts (Graff *et al.*, 2016). This is mainly due to two factors: lower nutrient availability in natural environments limits growth and therefore the need for high energy acquisition and resource allocation to pigment synthesis; and highly variable natural light conditions favor phenotypes with fewer pigments. Although not explored in our work, nutrient availability probably exerts a major influence on the pigment phenotype and absorption properties of *M. rubrum*, as it has been

observed in cryptophytes (Sciandra *et al.*, 2000). It is therefore very much possible that the pigment phenotypes of individual cells evolve with time, according to changes in light or nutrient availability, hence modifying the optical properties of the entire bloom. Additionally, seawater temperature measured on site shortly before the bloom (24 March 2021) was significantly lower ( $11.8^\circ\text{C}$ ; Quadri Database, 2023) than those at which *M. rubrum* cells were cultivated in our experiments ( $17.5$  and  $21^\circ\text{C}$ ). As pigment content in phytoplankton generally decreases at lower temperatures (Hammer *et al.*, 2002), this can also contribute to the less-pigmented phenotype observed in the bloom.

### Remote sensing of *M. rubrum* blooms

As previously mentioned, changes in the optical properties of individual cells can play a role in driving seawater optical variability in the case of red tides dominated by a given species. In particular, variability in the chl *a*-specific absorption coefficient is an important source of uncertainty in the estimation of [chl *a*] from satellite remote sensing, as  $a_{\text{phy}}^*(665)$  is a key parameter in bio-optical algorithms based on reflectance inversion (Gons *et al.*, 2002; Bricaud *et al.*, 2004; Gilerson *et al.*, 2010; Zheng and DiGiacomo, 2017). For example, a recent study demonstrated that satellite measurement of [chl *a*] was improved when using a variable  $a_{\text{phy}}^*(665)$  model rather than a fixed coefficient (Bramich *et al.*, 2021). The lab and field data presented here offer an opportunity to appraise the influence of photoacclimation-related changes in  $a_{\text{phy}}^*(665)$  on the estimation of [chl *a*] by satellite remote sensing during a *M. rubrum* red tide. Although the lower values of the  $a_{\text{phy}}^*(665)$  envelope correspond to extremely pigmented phenotypes that are less likely to

occur in natural environments (Graff et al., 2016), our results suggest that [chl *a*] retrieval can be underestimated by about 30% due to photoacclimation (Fig. 7D) if we consider the upper lab-measured  $a_{\text{phy}}^*(665)$  as plausible.

The map of the bloom on 27 March 2021 (Fig. 8A) illustrates the spatial heterogeneity of *M. rubrum* blooms (Crawford, 1989), with patches of high [chl *a*] stretching in narrow filament-like structures. These structures probably result mainly from hydrodynamics (Packard et al., 1978) and to a lesser extent from the aggregation of the ciliates due to their motility. The map also shows important [chl *a*] reaching  $250 \text{ mg}\cdot\text{m}^{-3}$ , highlighting the ability of *M. rubrum* blooms to reach high biomasses, although values four times higher have been observed (Smith Jr. and Barber, 1979). The second image on 29 March 2021 (Fig. 8B) shows the rapid evolution of the bloom during a short period of 2 days. The maximal [chl *a*] is drastically reduced, and the spatial distribution of the bloom greatly modified, with a few patches located closer to land. The rapid reduction in surface [chl *a*] observed in our study can be explained by a reduction in phytoplanktonic growth combined with increased losses. First, intra-specific competition for prey or nutrients may constitute a significant limitation to growth during the late stages of massive *M. rubrum* blooms, as starvation in ciliate populations rapidly leads to reduced growth rates (Kim et al., 2017). Then, loss in ciliate biomass may have been caused by a combination of physical dispersal of the plankton by currents (both horizontal and vertical), migration of *M. rubrum* cells to deeper waters, and grazing by meso- or microzooplankton. Additionally, the role of parasites and viruses, that have been shown to exert strong control on phytoplankton populations (Chambouvet et al., 2008; Biggs et al., 2021), cannot be ruled out in the case of *M. rubrum* (Crawford et al., 1997). Satellite remote sensing studies on the relation between local-scale hydrodynamics and the spatial structure of *M. rubrum* blooms, as well as field surveys of primary production and composition of the planktonic community during bloom events, would help elucidate the respective contributions of these phenomena to the bloom's distribution and decline.

### Methodological bottlenecks and perspectives for the study of *M. rubrum* in natural environments

*M. rubrum* has sometimes been poorly represented in traditional surveys of planktonic communities, because of its rather confusing trophic position between phytoplankton and microzooplankton, and of its fragility with regard to traditional methods of phytoplankton collection and preservation. Thus, its contribution to primary production has probably been underestimated in a number of studies (Crawford, 1989). The pertinence of including *Mesodinium* as a genus of interest in field surveys has since been recognized, notably in the light of its trophic interaction with the toxic dinoflagellate *Dinophysis* (Harred and Campbell, 2014). In the absence of quantitative microscopic observation or imaging data, alloxanthin concentration (or alloxanthin/chl *a* ratio) can also be a good indicator of the presence or abundance of *M. rubrum*, although not self-sufficient as it is impossible to discriminate between *M. rubrum* and cryptophytes based on this pigment alone. Alloxanthin is the specific pigment of cryptophytes, used in CHEMTAX analyses to assess the contribution of cryptophytes to the phytoplankton biomass. As noted by

Llewellyn et al. (2005), seasonal *M. rubrum* blooms could periodically constitute a significant part of the cryptophyte-chl *a* inferred from such methods. Inversely, the similarity in pigment content and optical properties means that cryptophyte red tides observed on satellite images could also be misidentified as *M. rubrum*. This highlights the importance of confirming the identity of the causative organism of a red tide (via microscopic observation) whenever possible.

Phycocerythrin 545 is even more specific to *M. rubrum* and its cryptophyte prey, as it is only produced by certain cryptophyte genera, including those upon which *M. rubrum* acquires its plastids (Altenburger et al., 2020). Despite this, PE 545 has rarely been measured when studying the pigments of *M. rubrum* (Rial et al., 2013; Gaillard et al., 2020), especially when it comes to field studies (Dierssen et al., 2015; Guzmán et al., 2016; this study). Indeed, this protein presents a series of constraints and limitations for its accurate quantification. First, due to its hydrophilic nature, it is not extracted and eluted along the chlorophylls and carotenoids, and hence not measured with classical HPLC protocols. It is therefore necessary to collect extra samples specifically for this pigment. However, as was demonstrated by Lawrenz et al. (2011) and confirmed by experiments conducted by us prior to this study (Fig. S3), it is not possible to efficiently recover PBPs from samples filtered on glass fiber filters, contrary to lipophilic pigments. This could be due to a strong binding of PBPs with the glass fibers, preventing any further extraction in aqueous solvents. This hypothesis is supported by the fact that PE 545 is visibly present on GF/F filters, that show a bright pink coloration on the back side, but cannot be extracted (Fig. S3). This also poses a problem for the analysis of absorption spectra with the filter-pad technique, as the specific absorption peak of PE 545 is significantly reduced (Fig. 4).

Moreover, the traditional filter pad technique seems to reach some limits when it comes to precise measurements of specific absorption coefficients. Measurements of microalgal absorption performed using filter pads often give strangely high  $a_{\text{phy}}^*(665)$  values, as noted by Zheng and DiGiacomo (2017). This was also the case in our study, with measurements of  $a_{\text{phy}}^*(665)$  flirting with or going beyond the theoretical limit of absorption of dissolved chl *a* in seawater (Fig. S5B). While Zheng and DiGiacomo (2017) mention that the absorption of chlorophyll *b* at 665 nm could contribute to these high  $a_{\text{phy}}^*(665)$  values, HPLC analysis of our bloom samples did not reveal any chl *b*, ruling this explanation out. Bricaud et al. (2004) discussed a similar phenomenon with the chl *a*-specific absorption coefficients at 440 nm they observed in many samples from various oceanographic cruises. The mismatch between the absorption values measured with filter pads or modeled from *in situ* reflectance in our study also illustrates the apparent overestimation of absorption occurring with the filter pad technique. While the explanations for this phenomenon remain unclear, we argue that this uncertainty in absorption measurements is problematic, in particular as more *in situ* measurements of *M. rubrum* blooms are needed to better characterize the range of absorption properties of this ciliate in different environments.

Methods for studying *M. rubrum* blooms in the field should take these considerations into account, as well as adapt to the peculiarities of PBPs and to the fragility of the ciliate. For

absorption measurements, nondestructive methods should be preferred whenever possible. For example, using a point-source integrating-cavity absorption meter (PSICAM, Röttgers *et al.*, 2007) for *in situ* measurements could be promising, as this device is adapted to the relatively low cell densities in the field and overcomes the measurement issues caused by glass fiber filters. To collect samples for PE 545 measurements, concentrating the algal biomass by filtering seawater on hydrophobic polycarbonate filters could be envisioned, though this method still needs to be thoroughly tested. Another option would be to sample relatively small volumes of seawater for centrifugation and quantify PE 545 through fluorescence measurement rather than absorption, as the former is much more sensitive and requires less biomass. Such a protocol would nonetheless require prior appropriate calibration.

The importance of PE 545 for *M. rubrum* ecophysiology should motivate such investigations toward measurements in natural environments. Moreover, this pigment is responsible for the characteristic shape of the reflectance spectrum of *M. rubrum* blooms, with low reflectance in the green spectral region (Gernez *et al.*, 2023). Knowledge about PE 545 optical properties *in situ* is therefore determinant for developing remote-sensing algorithms designed to accurately detect and characterize *M. rubrum* blooms. High-resolution satellite remote sensing is indeed a promising tool for studying these periodical, ecologically important phenomena in coastal waters (Dierssen *et al.*, 2015; Gernez *et al.*, 2023).

## CONCLUSIONS

The kleptoplastidic ciliate *M. rubrum* shows classical photoacclimation responses similar to that of its cryptophyte prey. Different pigment phenotypes in *M. rubrum* induce variability in its absorption properties, including the chl *a*-specific absorption coefficient that is used in chl *a*-estimation algorithms from remote sensing reflectance. High-resolution satellite remote sensing of a coastal red tide shows that *M. rubrum* forms concentrated patches of cells that stretch over several kilometers, and that the spatial structure and chl *a* biomass of the bloom change rapidly over a short period of 2 days. Overall, these results shed light on the ecophysiology of *M. rubrum*, a peculiar mixotrophic ciliate with a high degree of specialization toward photosynthesis. Future studies will have to overcome technical challenges to better characterize the physiology and pigment composition of this ecologically important ciliate during blooms in natural environments.

## ACKNOWLEDGEMENTS

We are grateful to Dr David Jaén (LCCRRPP, Junta de Andalucía, Spain) for generously sharing his cultures of *Teleaulax amphiox-ia* (AND-A0710) and Dr Per Juel Hansen (marine Biological Station, University of Copenhagen, Helsingør, Denmark) for his strain of *M. rubrum* (MrDK-2009). We sincerely thank Florian Massuyeau (Institut des Matériaux-Jean Rouxel, Nantes Université, France) for letting us use the dual beam UV–Vis–NIR spectrophotometer at his institute, and for helping us with measurements. Thank you to Aurélie Charrier, Virginie Raimbault, Marie Engel and Léna Gouhier (PHYTOX Physalg, IFREMER

Nantes) for their help during culture work, and Elise Robert (PHYTOX Genalg, IFREMER Nantes) for pigment analysis. We sincerely thank Christophe Six and Sarah Garric of the Station Biologique de Roscoff for their helpful insights and comments on a previous version of this work. We thank two anonymous reviewers for their critical and relevant comments on the first version of this manuscript. Finally, we thank the French taxpayers for supporting this research through our salaries and public funding of project LASHA (CNES).

## FUNDING

Centre National d'Etudes Spatiales (CNES, France).

## SUPPLEMENTARY DATA

Supplementary data is available at *Journal of Plankton Research* online.

## DATA AVAILABILITY

A github repository with all the R scripts used to analyze data presented in this study, as well as the associated raw data, is available at <https://github.com/vpochic/photoacclim2.0>. Data absent from the repository (satellite images) are available upon request.

## REFERENCES

- Altenburger, A., Blossom, H. E., Garcia-Cuetos, L., Jakobsen, H. H., Carstensen, J., Lundholm, N., Hansen, P. J., Moestrup, Ø. *et al.* (2020) Dimorphism in cryptophytes—the case of *Teleaulax amphiox-ia*/*Plagioselmis prolunga* and its ecological implications. *Sci. Adv.*, **6**, eabb1611. <https://doi.org/10.1126/sciadv.abb1611>.
- Altenburger, A., Cai, H., Li, Q., Drumm, K., Kim, M., Zhu, Y., Garcia-Cuetos, L., Zhan, X. *et al.* (2021) Limits to the cellular control of sequestered cryptophyte prey in the marine ciliate *Mesodinium rubrum*. *ISME J.*, **15**, 1056–1072. <https://doi.org/10.1038/s41396-020-00830-9>.
- Barber, R. T., White, A. W. and Siegelman, H. W. (1969) Evidence for a cryptomonad symbiont in the ciliate, *Cyclotrichium meunieri*. *J. Phycol.*, **5**, 86–88. <https://doi.org/10.1111/j.1529-8817.1969.tb02583.x>.
- Biggs, T. E. G., Huisman, J. and Brussaard, C. P. D. (2021) Viral lysis modifies seasonal phytoplankton dynamics and carbon flow in the Southern Ocean. *ISME J.*, **15**, 3615–3622. <https://doi.org/10.1038/s41396-021-01033-6>.
- Bramich, J., Bolch, C. J. and Fischer, A. (2021) Improved red-edge chlorophyll-*a* detection for Sentinel 2. *Ecol. Indic.*, **120**, 106876. <https://doi.org/10.1016/j.ecolind.2020.106876>.
- Bricaud, A. and Stramski, D. (1990) Spectral absorption coefficients of living phytoplankton and nonalgal biogenous matter: a comparison between the Peru upwelling area and the Sargasso Sea. *Limnol. Oceanogr.*, **35**, 562–582. <https://doi.org/10.4319/lo.1990.35.3.0562>.
- Bricaud, A., Babin, M., Morel, A. and Claustre, H. (1995) Variability in the chlorophyll-specific absorption coefficients of natural phytoplankton: analysis and parameterization. *J. Geophys. Res.*, **100**, 13321–13332. <https://doi.org/10.1029/95JC00463>.
- Bricaud, A., Claustre, H., Ras, J. and Oubelkheir, K. (2004) Natural variability of phytoplanktonic absorption in oceanic waters: influence of the size structure of algal populations. *J. Geophys. Res.: Oceans*, **109**, C11010. <https://doi.org/10.1029/2004JC002419>.
- Caballero, I., Fernández, R., Escalante, O. M., Mamán, L. and Navarro, G. (2020) New capabilities of Sentinel-2A/B satellites combined with *in situ* data for monitoring small harmful algal blooms in complex coastal waters. *Sci. Rep.*, **10**, 8743. <https://doi.org/10.1038/s41598-020-65600-1>.

- Chambouvet, A., Morin, P., Marie, D. and Guillou, L. (2008) Control of toxic marine dinoflagellate blooms by serial parasitic killers. *Science*, **322**, 1254–1257. <https://doi.org/10.1126/science.1164387>.
- Craig, S. E., Lohrenz, S. E., Lee, Z., Mahoney, K. L., Kirkpatrick, G. J., Schofield, O. M. and Steward, R. G. (2006) Use of hyperspectral remote sensing reflectance for detection and assessment of the harmful alga, *Karenia brevis*. *Appl. Opt.*, **45**, 5414–5425. <https://doi.org/10.1364/AO.45.005414>.
- Crawford, D. (1989) *Mesodinium rubrum*: the phytoplankton that wasn't. *Mar. Ecol. Prog. Ser.*, **58**, 161–174. <https://doi.org/10.3354/meps058161>.
- Crawford, D. W., Purdie, D. A., Lockwood, A. P. M. and Weissman, P. (1997) Recurrent red-tides in the Southampton water estuary caused by the phototrophic ciliate *Mesodinium rubrum*. *Estuar. Coast. Shelf Sci.*, **45**, 799–812. <https://doi.org/10.1006/ecss.1997.0242>.
- Cunningham, B. R., Greenwold, M. J., Lachenmyer, E. M., Heidenreich, K. M., Davis, A. C., Dudycha, J. L. and Richardson, T. L. (2019) Light capture and pigment diversity in marine and freshwater cryptophytes. *J. Phycol.*, **55**, 552–564. <https://doi.org/10.1111/jpy.12816>.
- Darwin, C. (1839) *Voyage of the Beagle*, Penguin Books, London, England.
- Denman, K. L. and Gargett, A. E. (1983) Time and space scales of vertical mixing and advection of phytoplankton in the upper ocean. *Limnol. Oceanogr.*, **28**, 801–815. <https://doi.org/10.4319/lo.1983.28.5.0801>.
- Díaz, P. A., Ruiz-Villarreal, M., Mouriño-Carballido, B., Fernández-Pena, C., Riobó, P. and Reguera, B. (2019) Fine scale physical-biological interactions during a shift from relaxation to upwelling with a focus on *Dinophysis acuminata* and its potential ciliate prey. *Prog. Oceanogr.*, **175**, 309–327. <https://doi.org/10.1016/j.pocean.2019.04.009>.
- Dierssen, H., McManus, G. B., Chlus, A., Qiu, D., Gao, B.-C. and Lin, S. (2015) Space station image captures a red tide ciliate bloom at high spectral and spatial resolution. *Proc. Natl. Acad. Sci. USA*, **112**, 14783–14787. <https://doi.org/10.1073/pnas.1512538112>.
- Dolan, J. R. and Marrasé, C. (1995) Planktonic ciliate distribution relative to a deep chlorophyll maximum: Catalan Sea, N.W. Mediterranean, June 1993. *Deep-Sea Res. I Oceanogr. Res. Pap.*, **42**, 1965–1987. [https://doi.org/10.1016/0967-0637\(95\)00092-5](https://doi.org/10.1016/0967-0637(95)00092-5).
- Doust, A. B., Marai, C. N. J., Harrop, S. J., Wilk, K. E., Curmi, P. M. G. and Scholes, G. D. (2004) Developing a structure–function model for the Cryptophyte Phycoerythrin 545 using ultrahigh resolution crystallography and ultrafast laser spectroscopy. *J. Mol. Biol.*, **344**, 135–153. <https://doi.org/10.1016/j.jmb.2004.09.044>.
- Fenchel, T. and Hansen, P. J. (2006) Motile behaviour of the bloom-forming ciliate *Mesodinium rubrum*. *Mar. Biol.*, **2**, 33–40. <https://doi.org/10.1080/17451000600571044>.
- Gaillard, S., Charrier, A., Malo, F., Carpentier, L., Bougaran, G., Hégaret, H., Réveillon, D., Hess, P. et al. (2020) Combined effects of temperature, irradiance, and pH on *Teleaulax amphioxeia* (Cryptophyceae) physiology and feeding ratio for its predator *Mesodinium rubrum* (Ciliophora)1. *J. Phycol.*, **56**, 775–783. <https://doi.org/10.1111/jpy.12977>.
- Garnier, S., Ross, N., Rudis, R., Camargo, P. A., Sciani, M. and Scherer, C. (2023) *Viridis(Lite) - Colorblind-Friendly Color Maps for R*. doi: <https://doi.org/10.5281/zenodo.4678327>, viridisLite package version 0.4.2, <https://sjmgarnier.github.io/viridis/>.
- Gernez, P., Doxaran, D. and Barillé, L. (2017) Shellfish aquaculture from space: potential of Sentinel2 to monitor tide-driven changes in turbidity, chlorophyll concentration and oyster physiological response at the scale of an oyster farm. *Front. Mar. Sci.*, **4**, 137. <https://doi.org/10.3389/fmars.2017.00137>.
- Gernez, P., Zoffoli, M. L., Lacour, T., Hernandez Fariñas, T., Navarro, G., Caballero, I. and Harmel, T. (2023) The many shades of red tides: Sentinel-2 optical types of highly-concentrated harmful algal blooms. *Remote Sens. Environ.*, **287**, 113486. <https://doi.org/10.1016/j.rse.2023.113486>.
- Gilerson, A. A., Gitelson, A. A., Zhou, J., Gurlin, D., Moses, W., Ioannou, I. and Ahmed, S. A. (2010) Algorithms for remote estimation of chlorophyll-*a* in coastal and inland waters using red and near infrared bands. *Opt. Express*, **18**, 24109–24125. <https://doi.org/10.1364/OE.18.024109>.
- Gomori, G. (1955) Preparation of buffers for use in enzyme studies. In Abelson, J. N., Simon, M. I. (eds), *Methods in Enzymology*. Academic Press, Cambridge, MA, U.S. pp. 138–146. [https://doi.org/10.1016/0076-6879\(55\)01020-3](https://doi.org/10.1016/0076-6879(55)01020-3).
- Gons, H. J. (1999) Optical tele-detection of chlorophyll *a* in turbid inland waters. *Environ. Sci. Technol.*, **33**, 1127–1132. <https://doi.org/10.1021/es9809657>.
- Gons, H. J., Rijkeboer, M. and Ruddick, K. G. (2002) A chlorophyll-retrieval algorithm for satellite imagery (medium resolution imaging spectrometer) of inland and coastal waters. *J. Plankton Res.*, **24**, 947–951. <https://doi.org/10.1093/plankt/24.9.947>.
- Graff, J. R., Westberry, T. K., Milligan, A. J., Brown, M. B., Dall'Olmo, G., Reifel, K. M. and Behrenfeld, M. J. (2016) Photoacclimation of natural phytoplankton communities. *Mar. Ecol. Prog. Ser.*, **542**, 51–62. <https://doi.org/10.3354/meps11539>.
- Guillard, R. R. L. and Hargraves, P. E. (1993) *Stichochrysis immobilis* is a diatom, not a chrysophyte. *Phycologia*, **32**, 234–236. <https://doi.org/10.2216/i0031-8884-32-3-234.1>.
- Guillotreau, P., Bihan, V. L., Morineau, B. and Pardo, S. (2021) The vulnerability of shellfish farmers to HAB events: an optimal matching analysis of closure decrees. *Harmful Algae*, **101**, 101968. <https://doi.org/10.1016/j.hal.2020.101968>.
- Gustafson, D. E., Stoecker, D. K., Johnson, M. D., Van Heukelem, W. F. and Sneider, K. (2000) Cryptophyte algae are robbed of their organelles by the marine ciliate *Mesodinium rubrum*. *Nature*, **405**, 1049–1052. <https://doi.org/10.1038/35016570>.
- Guzmán, L., Varela, R., Muller-Karger, F. and Lorenzoni, L. (2016) Bio-optical characteristics of a red tide induced by *Mesodinium rubrum* in the Cariaco Basin, Venezuela. *J. Mar. Syst.*, **160**, 17–25. <https://doi.org/10.1016/j.jmarsys.2016.03.015>.
- Hammer, A., Schumann, R. and Schubert, H. (2002) Light and temperature of *Rhodomonas salina* (Cryptophyceae): photosynthetic performance. *Aquat. Microb. Ecol.*, **29**, 287–296. <https://doi.org/10.3354/ame029287>.
- Harmel, T., Chami, M., Tormos, T., Reynaud, N. and Danis, P.-A. (2018) Sun-glint correction of the multi-spectral instrument (MSI)-SENTINEL-2 imagery over inland and sea waters from SWIR bands. *Remote Sens. Environ.*, **204**, 308–321. <https://doi.org/10.1016/j.rse.2017.10.022>.
- Harred, L. B. and Campbell, L. (2014) Predicting harmful algal blooms: a case study with *Dinophysis ovum* in the Gulf of Mexico. *J. Plankton Res.*, **36**, 1434–1445. <https://doi.org/10.1093/plankt/fbu070>.
- Hart, T. J. (1943) Darwin and 'water-bloom'. *Nature*, **152**, 661–662. <https://doi.org/10.1038/152661b0>.
- Heidenreich, K. M. and Richardson, T. L. (2020) Photopigment, absorption, and growth responses of marine Cryptophytes to varying spectral irradiance. *J. Phycol.*, **56**, 507–520. <https://doi.org/10.1111/jpy.12962>.
- Hernández-Urcera, J., Rial, P., García-Portela, M., Lourés, P., Kilcoyne, J., Rodríguez, F., Fernández-Villamarín, A. and Reguera, B. (2018) Notes on the cultivation of two mixotrophic *Dinophysis* species and their ciliate prey *Mesodinium rubrum*. *Toxins*, **10**, 505. <https://doi.org/10.3390/toxins10120505>.
- van den Hoff, J. and Bell, E. (2015) The ciliate *Mesodinium rubrum* and its cryptophyte prey in Antarctic aquatic environments. *Polar Biol.*, **38**, 1305–1310. <https://doi.org/10.1007/s00300-015-1686-z>.
- Jaubert, M., Bouly, J.-P., Ribera d'Alcalá, M. and Falcatore, A. (2017) Light sensing and responses in marine microalgae. *Curr. Opin. Plant Biol.*, **37**, 70–77. <https://doi.org/10.1016/j.pbi.2017.03.005>.
- Johnson, M. D. and Stoecker, D. K. (2005) Role of feeding in growth and photophysiology of *Myrionecta rubra*. *Aquat. Microb. Ecol.*, **39**, 303–312. <https://doi.org/10.3354/ame039303>.
- Johnson, M. D., Stoecker, D. K. and Marshall, H. G. (2013) Seasonal dynamics of *Mesodinium rubrum* in Chesapeake Bay. *J. Plankton Res.*, **35**, 877–893. <https://doi.org/10.1093/plankt/ftb028>.

- Johnson, M. D., Moeller, H. V., Paight, C., Kellogg, R. M., McIlvin, M. R., Saito, M. A. and Lasek-Nesselquist, E. (2023) Functional control and metabolic integration of stolen organelles in a photosynthetic ciliate. *Curr. Biol.*, **33**, 973–980.e5. <https://doi.org/10.1016/j.cub.2023.01.027>.
- Kassambara, A. (2023) *Ggpubr: 'ggplot2' Based Publication Ready Plots*. R package version 0.6.0, <https://rpkgs.datanovia.com/ggpubr/>
- Kim, M., Drumm, K., Daugbjerg, N. and Hansen, P.J. (2017) Dynamics of sequestered cryptophyte nuclei in *Mesodinium rubrum* during starvation and refeeding. *Front. Microbiol.*, **8**, 423. <https://doi.org/10.3389/fmicb.2017.00423>.
- Lacour, L., Ardyna, M., Stec, K. F., Claustre, H., Prieur, L., Poteau, A., Ribera, d'Alcala, M. and Iudicone, D. (2017) Unexpected winter phytoplankton blooms in the North Atlantic subpolar gyre. *Nat. Geosci.*, **10**, 836–839. <https://doi.org/10.1038/ngeo3035>.
- Laviale, M. and Neveux, J. (2011) Relationships between pigment ratios and growth irradiance in 11 marine phytoplankton species. *Mar. Ecol. Prog. Ser.*, **425**, 63–77. <https://doi.org/10.3354/meps09013>.
- Lawrenz, E., Fedewa, E. J. and Richardson, T. L. (2011) Extraction protocols for the quantification of phycobilins in aqueous phytoplankton extracts. *J. Appl. Phycol.*, **23**, 865–871. <https://doi.org/10.1007/s10811-010-9600-0>.
- Leong, S. C. Y. and Taguchi, S. (2006) Detecting the bloom-forming dinoflagellate *Alexandrium tamarense* using the absorption signature. *Hydrobiologia*, **568**, 299–308. <https://doi.org/10.1007/s10750-006-0202-4>.
- Llewellyn, C. A., Fishwick, J. R. and Blackford, J. C. (2005) Phytoplankton community assemblage in the English Channel: a comparison using chlorophyll *a* derived from HPLC-CHEMTAX and carbon derived from microscopy cell counts. *J. Plankton Res.*, **27**, 103–119. <https://doi.org/10.1093/plankt/fbh158>.
- MacColl, R., Berns, D. S. and Gibbons, O. (1976) Characterization of cryptomonad phycoerythrin and phycocyanin. *Arch. Biochem. Biophys.*, **177**, 265–275. [https://doi.org/10.1016/0003-9861\(76\)90436-7](https://doi.org/10.1016/0003-9861(76)90436-7).
- MacIntyre, H. L., Kana, T. M., Anning, T. and Geider, R. J. (2002) Photoacclimation of photosynthesis irradiance response curves and photosynthetic pigments in microalgae and cyanobacteria. *J. Phycol.*, **38**, 17–38. <https://doi.org/10.1046/j.1529-8817.2002.00094.x>.
- Mafra, L. L., Nolli, P. K. W., Mota, L. E., Domit, C., Soeth, M., Luz, L. F. G., Sobrinho, B. F., Leal, J. G. *et al.* (2019) Multi-species okadaic acid contamination and human poisoning during a massive bloom of *Dinophysis acuminata* complex in southern Brazil. *Harmful Algae*, **89**, 101662. <https://doi.org/10.1016/j.hal.2019.101662>.
- Mendes, C. R. B., Costa, R. R., Ferreira, A., Jesus, B., Tavano, V. M., Dotto, T. S., Leal, M. C., Kerr, R. *et al.* (2023) Cryptophytes: an emerging algal group in the rapidly changing Antarctic peninsula marine environments. *Glob. Chang. Biol.*, **29**, 1791–1808. <https://doi.org/10.1111/gcb.16602>.
- Minnhagen, S., Kim, M., Salomon, P. S., Yih, W., Granéli, E. and Park, M. G. (2011) Active uptake of kleptoplastids by *Dinophysis caudata* from its ciliate prey *Myrionecta rubra*. *Aquat. Microb. Ecol.*, **62**, 99–108. <https://doi.org/10.3354/ame01459>.
- Moeller, H. V., Johnson, M. D. and Falkowski, P. G. (2011) Photoacclimation in the phototrophic marine ciliate *Mesodinium rubrum* (Ciliophora). *J. Phycol.*, **47**, 324–332. <https://doi.org/10.1111/j.1529-8817.2010.00954.x>.
- Morel, A. and Bricaud, A. (1981) Theoretical results concerning light absorption in a discrete medium, and application to specific absorption of phytoplankton. *Deep-Sea Res.*, **28**, 1375–1393. [https://doi.org/10.1016/0198-0149\(81\)90039-X](https://doi.org/10.1016/0198-0149(81)90039-X).
- Morel, A. and Prieur, L. (1977) Analysis of variations in ocean color. *Limnol. Oceanogr.*, **22**, 709–722. <https://doi.org/10.4319/lo.1977.22.4.0709>.
- Mueller, J. L. (2003) In-water radiometric profile measurements and data analysis protocols. In Fargion, G. S., McClain, C. R. and Mueller, J. L. (eds.), *Ocean Optics Protocols for Satellite Ocean Color Sensor Validation, Revision 4. Volume III: Radiometric Measurements and Data Analysis Protocols*. National Aeronautics and Space Administration, Goddard Space Flight Center, Greenbelt, MD, U.S. <https://doi.org/10.25607/OBP-62>
- Overkamp, K. E., Gasper, R., Kock, K., Herrmann, C., Hofmann, E. and Frankenberg-Dinkel, N. (2014) Insights into the biosynthesis and assembly of Cryptophyceyan Phycobiliproteins. *J. Biol. Chem.*, **289**, 26691–26707. <https://doi.org/10.1074/jbc.M114.591131>.
- Packard, T. T., Blasco, D. and Barber, R. T. (1978) *Mesodinium rubrum* in the Baja California upwelling system. In Boje, R. and Tomczak, M. (eds.), *Upwelling Ecosystems*. Springer, Berlin, Heidelberg, pp. 73–89. [https://doi.org/10.1007/978-3-642-66985-9\\_7](https://doi.org/10.1007/978-3-642-66985-9_7)
- Park, M. G., Kim, S., Kim, H. S., Myung, G., Kang, Y. G. and Yih, W. (2006) First successful culture of the marine dinoflagellate *Dinophysis acuminata*. *Aquat. Microb. Ecol.*, **45**, 101–106. <https://doi.org/10.3354/ame045101>.
- Peltomaa, E. and Johnson, M. D. (2017) *Mesodinium rubrum* exhibits genus-level but not species-level cryptophyte prey selection. *Aquat. Microb. Ecol.*, **78**, 147–159. <https://doi.org/10.3354/ame01809>.
- Quadrige (2023) *Données Par paramètre*. Quadrige (Ifremer). <https://doi.org/10.12770/cf5048f6-5bbf-4e44-ba74-e6f429af51ea>
- R Core Team. (2022) *R: A Language and Environment for Statistical Computing*. R Foundation for Statistical Computing, Vienna, Austria. URL <https://www.R-project.org/>
- Rial, P., Garrido, J. L., Jaén, D. and Rodríguez, F. (2013) Pigment composition in three *Dinophysis* species (Dinophyceae) and the associated cultures of *Mesodinium rubrum* and *Teleaulax amphioxeia*. *J. Plankton Res.*, **35**, 433–437. <https://doi.org/10.1093/plankt/fbs099>.
- Richardson, T. L. (2022) The colorful world of cryptophyte phycobiliproteins. *J. Plankton Res.*, **44**, 806–818. <https://doi.org/10.1093/plankt/fbac048>.
- Roesler, C., Stramski, D., D'Sa, E. J., Röttgers, R. and Reynolds, R. A. (2018) Chapter 5: spectrophotometric measurements of particulate absorption using filter pads. In Neeley, A. R. and Mannino, A. (eds.), *IOCCG Protocol Series (2018). Inherent Optical Property Measurements and Protocols: Absorption Coefficient*. IOCCG Ocean Optics and Biogeochemistry Protocols for Satellite Ocean Colour Sensor Validation, Dartmouth, NS, Canada. <https://doi.org/10.25607/OBP-119>
- Röttgers, R. and Gehnke, S. (2012) Measurement of light absorption by aquatic particles: improvement of the quantitative filter technique by use of an integrating sphere approach. *Appl. Opt.*, **51**, 1336–1351. <https://doi.org/10.1364/AO.51.001336>.
- Röttgers, R., Häse, C. and Doerffer, R. (2007) Determination of the particulate absorption of microalgae using a point-source integrating-cavity absorption meter: verification with a photometric technique, improvements for pigment bleaching, and correction for chlorophyll fluorescence. *Limnol. Oceanogr. Meth.*, **5**, 1–12. <https://doi.org/10.4319/lom.2007.5.1>.
- Ruddick, K. G., De Cauwer, V., Park, Y.-J. and Moore, G. (2006) Seaborne measurements of near infrared water-leaving reflectance: the similarity spectrum for turbid waters. *Limnol. Oceanogr.*, **51**, 1167–1179. <https://doi.org/10.4319/lo.2006.51.2.1167>.
- Sciandra, A., Lazzara, L., Claustre, H. and Babin, M. (2000) Responses of growth rate, pigment composition and optical properties of *Cryptomonas* sp. to light and nitrogen stresses. *Mar. Ecol. Prog. Ser.*, **201**, 107–120. <https://doi.org/10.3354/meps201107>.
- Six, C., Ratin, M., Marie, D. and Corre, E. (2021) Marine *Synechococcus* picocyanobacteria: Light utilization across latitudes. *Proc. Natl. Acad. Sci. USA*, **118**, e2111300118. <https://doi.org/10.1073/pnas.2111300118>.
- Smith, W. O. Jr. and Barber, R. T. (1979) A carbon budget for the autotrophic ciliate *Mesodinium rubrum*. *J. Phycol.*, **15**, 27–33. <https://doi.org/10.1111/j.1529-8817.1979.tb02957.x>.
- Spangler, L. C., Yu, M., Jeffrey, P. D. and Scholes, G. D. (2022) Controllable Phycobilin modification: an alternative photoacclimation response in cryptophyte algae. *ACS Cent. Sci.*, **8**, 340–350. <https://doi.org/10.1021/acscentsci.1c01209>.

- Stramski, D. and Mobley, C. D. (1997) Effects of microbial particles on oceanic optics: a database of single-particle optical properties. *Limnol. Oceanogr.*, **42**, 538–549. <https://doi.org/10.4319/lo.1997.42.3.0538>.
- Stramski, D., Rosenberg, G. and Legendre, L. (1993) Photosynthetic and optical properties of the marine chlorophyte *Dunaliella tertiolecta* grown under fluctuating light caused by surface-wave focusing. *Mar. Biol.*, **115**, 363–372. <https://doi.org/10.1007/BF00349833>.
- Stramski, D., Bricaud, A. and Morel, A. (2001) Modeling the inherent optical properties of the ocean based on the detailed composition of the planktonic community. *Appl. Opt.*, **40**, 2929–2945. <https://doi.org/10.1364/AO.40.002929>.
- Stramski, D., Sciandra, A. and Claustre, H. (2002) Effects of temperature, nitrogen, and light limitation on the optical properties of the marine diatom *Thalassiosira pseudonana*. *Limnol. Oceanogr.*, **47**, 392–403. <https://doi.org/10.4319/lo.2002.47.2.0392>.
- Stramski, D., Reynolds, R. A., Kaczmarek, S., Uitz, J. and Zheng, G. (2015) Correction of pathlength amplification in the filter-pad technique for measurements of particulate absorption coefficient in the visible spectral region. *Appl. Opt.*, **54**, 6763–6782. <https://doi.org/10.1364/AO.54.006763>.
- Thyng, K. M., Greene, C. A., Hetland, R. D., Zimmerle, H. M. and DiMarco, S. F. (2016) True Colors of oceanography: guidelines for effective and accurate Colormap selection. *Oceanography*, **29**, 9–13. <https://doi.org/10.5670/oceanog.2016.66>.
- Wickham, H. (2007) Reshaping data with the reshape package. *J. Stat. Softw.*, **21**, 1–20. <https://doi.org/10.18637/jss.v021.i12>.
- Wickham, H., Averick, M., Bryan, J., Chang, W., McGowan, L. D., François, R., Grolemund, G., Hayes, A. et al. (2019) Welcome to the Tidyverse. *J. Open Source Softw.*, **4**, 1686. <https://doi.org/10.21105/joss.01686>.
- Yih, W., Kim, H. S., Jeong, H. J., Myung, G. and Kim, Y. G. (2004) Ingestion of cryptophyte cells by the marine photosynthetic ciliate *Mesodinium rubrum*. *Aquat. Microb. Ecol.*, **36**, 165–170. <https://doi.org/10.3354/ame036165>.
- Zhao, K.-H., Porra, R. J. and Scheer, H. (2011) Phycobiliproteins. In Roy, S., Llewellyn, C. A., Egeland, E. S. and Johnsen, G. (eds.), *Phytoplankton Pigments: Characterization, Chemotaxonomy and Applications in Oceanography*. Cambridge University Press, Cambridge, England. <https://doi.org/10.1017/CBO9780511732263.014>.
- Zheng, G. and DiGiacomo, P. M. (2017) Remote sensing of chlorophyll-*a* in coastal waters based on the light absorption coefficient of phytoplankton. *Remote Sens. Environ.*, **201**, 331–341. <https://doi.org/10.1016/j.rse.2017.09.008>.